



Research paper

On the dependence of orientation averaging mean field homogenization on planar fourth-order fiber orientation tensors

Julian Karl Bauer^a, Thomas Böhlke^{b,*}^a Institute of Mechanics, Karlsruhe Institute of Technology (KIT), Germany^b Chair for Continuum Mechanics, Institute of Engineering Mechanics, Karlsruhe Institute of Technology (KIT), Germany

ARTICLE INFO

Keywords:

Fiber orientation tensor
Anisotropy
Elasticity
Small strain
Mean field homogenization
Fiber reinforced composites
Closure approximation

ABSTRACT

A comprehensive study on the influence of planar fourth-order fiber orientation tensors on effective linear elastic stiffnesses predicted by orientation averaging mean field homogenization is given. Fiber orientation states of sheet molding compound (SMC) are identified to be in most cases approximately planar. In the planar case, all possible fourth-order fiber orientation tensors are given by a minimal invariant set of structurally differing planar fourth-order fiber orientation tensors. This set defines a three-dimensional body and forms the basis for a comprehensive study on the influence of a fiber orientation distribution in terms of a fourth-order tensor on homogenized stiffnesses. The methodology of this study is the main contribution of this work and can be adopted to analyze the orientation dependence of any quantity which is a function of a planar fourth-order fiber orientation tensor. At specific points inside the set of planar fiber orientation tensors, effective stiffnesses are calculated with selected mean field homogenization schemes. These schemes are based on orientation averaging of transversely isotropic elasticity tensors following Advani and Tucker (1987), which is explicitly recast as linear invariant composition in the fiber orientation tensors of second and fourth order of Kanatani third kind. A maximum entropy reconstruction of a fiber orientation distribution function based on leading fiber orientation tensors, enables a new numerical formulation of the Advani and Tucker average for the special planar case. Polar plots of Young's modulus and generalized bulk modulus obtained by selected homogenization schemes are arranged on two-dimensional slices within the body of admissible fiber orientation tensors, visualizing the influence of the orientation tensor on the stiffness tensor. The orientation-dependence of the generalized bulk modulus differs significantly between selected homogenizations. Restrictions on the effective anisotropic material response caused by orthotropy of closure approximations are discussed.

1. Introduction

The effective mechanical properties of fiber reinforced composites highly depend on the microstructure. The microstructure descriptors fiber volume content and fiber orientation tensors are commonly used in homogenization techniques for two-phase composites (Buck et al., 2015; Brylka, 2017; Hessman et al., 2021; Schemmann et al., 2018b; Kehrer et al., 2020). Experimental or numerical identification and subsequent use of second-order fiber orientation tensors is well established in process chains (Görthofer et al., 2019) and commercial software. The use of higher-order fiber orientation tensors or the direct use of a fiber orientation distribution function, is progressing (Meyer et al., 2020). Nevertheless, closure approximations, which identify higher-order orientation information based on assumptions instead of information, are still used in material modeling. For the special case of linear elasticity, mean field homogenization is popular due to its

simplicity (Kehrer et al., 2020). A unified formulation of several mean field approximations is given in Hessman et al. (2021). The influence of model parameters, the fiber volume content or the aspect ratio of either the fiber's shape or the two-point correlation functions, on the predicted effective mechanical properties obtained by mean field homogenization, is studied extensively, e.g. in Kehrer et al. (2020), Buck et al. (2015), Brylka (2017), Hessman et al. (2021), Müller (2016), Trauth et al. (2021) and Kehrer (2019). However, the influence of fiber orientation distributions on the effective properties has not been studied systematically. In this work, the influence of fiber orientation distributions on the effective properties of long fiber reinforced composites with large aspect ratios, such as sheet molding compound (SMC), is studied. Fiber distributions of SMC are identified to be in most cases approximately planar and therefore correspond to fiber orientation tensors which are planar as well. A set of all admissible and structurally

* Correspondence to: Kaiserstraße 10, 76131 Karlsruhe, Chair for Continuum Mechanics, Institute of Engineering Mechanics, Karlsruhe Institute of Technology (KIT), Germany.

E-mail addresses: julian.bauer@kit.edu (J.K. Bauer), thomas.boehlke@kit.edu (T. Böhlke).

<https://doi.org/10.1016/j.mechmat.2022.104307>

Received 17 January 2022; Received in revised form 31 March 2022; Accepted 4 April 2022

Available online 22 April 2022

0167-6636/© 2022 The Authors. Published by Elsevier Ltd. This is an open access article under the CC BY license (<http://creativecommons.org/licenses/by/4.0/>).

differing planar fiber orientation tensors of fourth order is identified by Bauer and Böhlke (2021, 2022) within a three-dimensional framework. This set is the basis for a complete study on the influence of the fiber orientation distribution on the effective mechanical properties for selected orientation averaging mean field homogenizations within this work. This complete study is new and of high relevance as it visualizes all possible effective stiffness tensors which can be obtained for planar distributions and selected homogenizations. The methodology may be applied to any other homogenization or any effective quantity, which is a function of a planar fourth-order fiber orientation tensor. As a side effect, the limitations of the use of second-order orientation tensors only are visualized. The developed visualization method may be adopted to higher-dimensional parameter spaces of fourth-order fiber orientation tensors with lower symmetry.

This paper starts with definitions of fiber orientation tensors before orientation states of SMC specimen obtained by computer tomography (Pinter et al., 2018; Schöttl et al., 2020) are identified to be approximately planar. In consequence, the microstructure of SMC can be parameterized in the three-dimensional space of admissible planar fourth-order fiber orientation tensors. A parameterization of this space is obtained in Bauer and Böhlke (2021) and combined with a minimal parameter set of structurally distinct planar fourth-order fiber orientation tensors given in Bauer and Böhlke (2022). As the Advani–Tucker orientation average (Advani and Tucker III, 1987) is an essential building block of various mean field schemes, but the implication of its linearity in both the orientation tensor and the averaged quantity is seldomly addressed explicitly, a reformulation based on the harmonic decomposition (linear invariant decomposition) is given. A new numerical variant of the Advani–Tucker orientation average based on reconstructed FODF following the maximum entropy method, developed in Müller and Böhlke (2016) and Bauer and Böhlke (2022), is given and shown to have a good convergence for non-localized orientation states. In a next step, four mean field homogenization approximations (Kehrer et al., 2020; Walpole, 1966a,b; Benveniste, 1987) are reviewed, partially reformulated and investigated. Implementations are made available at Bauer (2022). The first approximations are orientation averaging Mori–Tanaka following Benveniste (1987) and a two step Hashin–Shtrikman homogenization scheme (Kehrer et al., 2020) both in formulations based on the orientation average following Advani and Tucker III (1987). The remaining two approximations are direct Advani–Tucker orientation averages of either a unidirectional stiffness or compliance obtained by the Mori–Tanaka (Mori and Tanaka, 1973) approximation. Views on the effective stiffnesses obtained by the selected schemes are given based on Young’s modulus and generalized bulk modulus following Böhlke and Brüggemann (2001). Observations on structural differences of the effective stiffnesses obtained by schemes averaging stiffness- or compliance-like quantities close this work.

Notation: Symbolic tensor notation is preferred in this paper. Tensors of first order are denoted by bold lowercase letters such as \mathbf{q} , \mathbf{n} , \mathbf{v} , \mathbf{e} . Tensors of second order are denoted by bold uppercase letters like \mathbf{N} or \mathbf{Q} and fourth-order tensors are denoted by, e.g., \mathbb{N} or \mathbb{D} . Tensors in representations for varying tensor order are represented by, e.g., $\mathbb{D}_{(k)}$, where k defines the tensor order. A linear mapping of a second-order by a fourth-order tensor reads as $\mathbf{A} = \mathbb{C}[\mathbf{B}]$. The scalar product reads as $\mathbf{A} \cdot \mathbf{B}$. The tensor power, i.e., the k th dyadic product of, e.g., a first order tensor \mathbf{a} is denoted by $\mathbf{a}^{\otimes k}$ yielding, e.g., $\mathbf{a}^{\otimes 3} = \mathbf{a} \otimes \mathbf{a} \otimes \mathbf{a}$. An orthonormal basis is denoted by $\{\mathbf{e}_i\}$ with $\mathbf{e}_i \cdot \mathbf{e}_j = \delta_{ij}$ and the Kronecker delta δ_{ij} . If a matrix of tensor coefficients is used in mixed notation, the coefficient matrix is directly followed by the tensor basis where the first index of the basis corresponds to the rows of the coefficients matrix, the second one to the columns. Summation convention applies, unless otherwise stated. Representations in index notation always refer to an orthonormal basis. The Rayleigh product is used to represent an active rotation of a physical quantity and for a first order tensor is defined by $\mathbf{Q} \star \mathbf{n} = n_i \mathbf{Q} \mathbf{e}_i$. Sets, i.e., collections of quantities, are denoted by calligraphic symbols, e.g., \mathcal{F} and are

constructed by curly braces. Inside the curly braces, elements of the set are given explicitly, or by a generator expression following the pattern {quantity|condition fulfilled inside set}. Although, this work and related code is based on Harris et al. (2020) and Meurer et al. (2017), numbering and indices follow the continuum mechanics convention starting at one.

2. On the dependence of orientation averaging mean field homogenization on planar fourth-order fiber orientation tensors

2.1. Sheet molding compound and planar microstructures

Sheet molding compound (SMC) is a material class with a thermoset polymer matrix enforced by long glass fibers and is of special interest in this work. Due to the manufacturing process (Böhlke et al., 2019), components made from SMC are shell-shaped, i.e., at each point of the component, the thickness is significantly smaller than the remaining two dimensions of the component. As the fiber length exceeds the component thickness, alignment of fibers perpendicular to the local plane of the shell is limited to local fiber bending. In consequence, local directional measures which describe the orientation of fibers in SMC components are approximately planar. In order to elaborate the consequences of this planarity, directional measures are introduced, closely following a more comprehensive discussion in Bauer and Böhlke (2021, sections 2.1 and 2.2).

A fiber orientation density function (FODF) is an established directional measure for the orientation of axisymmetric fibers contained inside a reference volume. Such a reference volume can be interpreted as a section of a structural component of specified size. The size of the reference volume influences the directional measurement and represents a scaling parameter in measurement algorithms, e.g., in Görthofer et al. (2019, Figure 4) or Schöttl et al. (2020). The FODF

$$\psi : S^2 \rightarrow \mathbb{R}, \quad \text{with } S^2 = \{\mathbf{n} \in \mathbb{R}^3 \mid \|\mathbf{n}\| = 1\} \quad (1)$$

at a given position inside a component maps any direction \mathbf{n} , being part of the two-dimensional surface of a unit sphere in three dimensions S^2 , onto a scalar value $\psi(\mathbf{n})$. The function $\psi(\mathbf{n})$ is non-negative, normalized and symmetric (see Advani and Tucker III, 1987; Bauer and Böhlke, 2021; Görthofer et al., 2020; Bauer and Böhlke, 2022). The FODF contains the complete directional information, which can be contained in a one-point correlation function, but is usually unknown. In contrast, orientation tensors only contain a limited amount of averaged information but can be obtained by computer tomography scans or flow simulations (Görthofer et al., 2019) and fit into the tensor framework of continuum mechanics. In this work, fiber orientation tensors of Kanatani (1984) first kind of second \mathbb{N} and fourth order \mathbb{N} are used and defined by

$$\mathbb{N} = \int_{S^2} \psi(\mathbf{n}) \mathbf{n} \otimes \mathbf{n} \, d\mathbf{n}, \quad (2)$$

$$\mathbb{N} = \int_{S^2} \psi(\mathbf{n}) \mathbf{n} \otimes \mathbf{n} \otimes \mathbf{n} \otimes \mathbf{n} \, d\mathbf{n}. \quad (3)$$

The fiber orientation tensors represent averaged directional measures and are coefficients of a three-dimensional tensorial Fourier series representation of the FODF

$$\psi(\mathbf{n}) = \frac{1}{4\pi} \sum_{k=0}^{\infty} \frac{2k+1}{2^k} \binom{2k}{k} \text{dev}(\mathbb{N}_{(k)}) \cdot \mathbf{n}^{\otimes k} \quad (4)$$

called spherical harmonic expansion (Kanatani, 1984, page 154), with the operator $\text{dev}(\cdot)$ extracting the deviatoric part, see Spencer (1970). Higher order fiber orientation tensors contain all tensors of lower order which implies $\mathbb{N} = \mathbb{N}[\mathbf{I}]$ for the tensor orders two and four, with the identity on second-order tensors $\mathbf{I} = \delta_{ij} \mathbf{e}_i \otimes \mathbf{e}_j$.

In order to define planarity of the directional measures, the basic properties of the second-order orientation tensor \mathbb{N} are briefly summarized following Bauer and Böhlke (2021). As \mathbb{N} is symmetric and

positive semi-definite, it can be diagonalized, i.e., pairs of eigenvalues λ_i with $\lambda_i \geq 0$ and orthonormal eigenvectors \mathbf{v}_i for $i \in [1, 2, 3]$ exist, such that

$$\mathbf{N} = N_{ij}^{(2)} \mathbf{e}_i \otimes \mathbf{e}_j = \sum_{i=1}^3 \lambda_i \mathbf{v}_i \otimes \mathbf{v}_i = \begin{bmatrix} \lambda_1 & 0 & 0 \\ & \lambda_2 & 0 \\ \text{sym} & & \lambda_3 \end{bmatrix} \mathbf{v}_i \otimes \mathbf{v}_j \quad (5)$$

holds with the ordering convention $\lambda_3 \leq \lambda_2 \leq \lambda_1$ and there exists a rotation defined by an orthogonal tensor

$$\mathbf{Q} = \mathbf{v}_i \otimes \mathbf{e}_i \quad (6)$$

mapping the arbitrary but fixed basis $\{\mathbf{e}_i\}$ onto the basis $\{\mathbf{v}_i\}$. A visual classification of structurally differing orientation tensors is given by the so called orientation triangle (Cintra and Tucker III, 1995; Chung and Kwon, 2002; Goldberg et al., 2017; Köbler et al., 2018). As $\lambda_3 = 1 - \lambda_1 - \lambda_2$ holds due to the normalization of ψ , any second-order orientation tensor can be represented by a pair (λ_1, λ_2) , which is connected to a point inside the orientation triangle and by a mapping \mathbf{Q} which defines the orthonormal basis $\{\mathbf{v}_i\}$ spanned by the eigenvectors. This basis is called orientation coordinate system (Bauer and Böhlke, 2021) and can be used to define the term planarity for FODF and fiber orientation tensors. A FODF is planar, if

$$\psi(\mathbf{n}(\varphi, \theta)) = 0 \quad \forall \varphi, \forall \theta \neq \frac{\pi}{2} \quad (7)$$

holds with a unit vector parameterized in two spherical angles in the orientation coordinate system

$$\mathbf{n}(\varphi, \theta) = \sin(\theta) \cos(\varphi) \mathbf{v}_1 + \sin(\theta) \sin(\varphi) \mathbf{v}_2 + \cos(\theta) \mathbf{v}_3. \quad (8)$$

A fiber orientation tensor of arbitrary order is planar if its successive contraction yields a second-order fiber orientation tensor with vanishing third eigenvalue.

The assumption of the planarity of SMC microstructures is assessed by inspection of a biaxial tensile specimen made of SMC. Second-order fiber orientation tensors following Eq. (5) at several locations inside this specimen are obtained by computer tomography following Schöttl et al. (2020) and are referenced as \mathcal{N}_{SMC}^{CT} . The obtained fiber orientation tensors are visualized as points inside an orientation triangle in Fig. 1. The orientation states along the upper right border of the triangle in Fig. 1 represent perfectly planar orientations, as the third eigenvalue $\lambda_3 = 1 - \lambda_1 - \lambda_2$ vanishes. The measured fiber orientation tensors align well onto the planar border of the orientation triangle in Fig. 1 and therefore confirm the planarity assumption. However, the spatial resolution of CT images as well as the choice of algorithm parameters for the processing of the CT images, influence the planarity of the resulting fiber orientation tensors. Not all fiber orientation tensors obtained for SMC in literature are perfectly planar. As an example, Kehrer et al. (2020, Figure 5) contains non-planar fiber orientation states, obtained by CT scans, indicating a high spatial resolution of the corresponding CT images combined with small extraction cylinders (see Görthofer et al., 2019, Figure 4) in the post-processing of the CT images. Visualizations of SMC microstructure data obtained by computer tomography (CT) are, e.g., given in Trauth et al. (2021, fig. 2). Artificially generated SMC microstructures can be found in Görthofer et al. (2020, fig. 3b and 5). The algorithm, which (Görthofer et al., 2020) used to generate artificial microstructures, hints towards the planarity of the resulting directional measures. Throughout this work, fiber orientation tensors of SMC are assumed to be perfectly planar and hence, the dependence of the mechanical response of shell-like SMC structures on a varying microstructure can be investigated based on planar fiber orientation tensors. In this work, the SMC-specific bundle structure which is, e.g., considered in Schöttl et al. (2021) and Görthofer et al. (2020), is not taken into account.

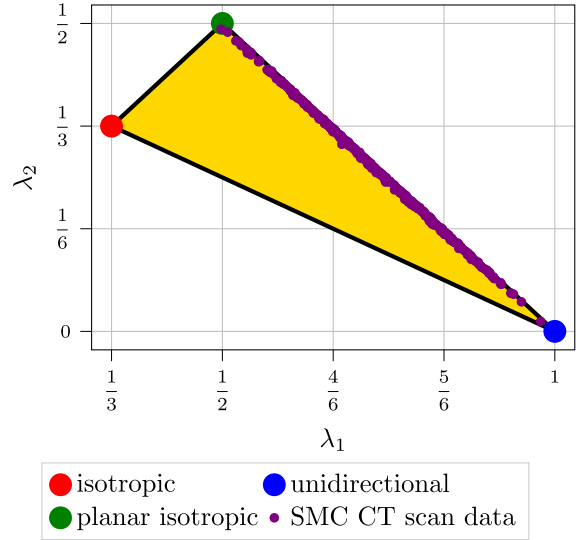


Fig. 1. Orientation triangle visualizing second-order orientation tensors \mathcal{N}_{SMC}^{CT} obtained by computer tomography (CT) scans at several positions of a SMC specimen. For reference, the vertices of the orientation triangle are labeled in the legend.

2.2. Planar fourth-order fiber orientation tensors

A parameterization of planar fiber orientation tensors of second order $\mathbb{N}^{\text{planar}}$ is given by

$$\begin{aligned} \mathbb{N}^{\text{planar}}(\lambda_1) &= \lambda_1 \mathbf{v}_1 \otimes \mathbf{v}_1 + (1 - \lambda_1) \mathbf{v}_2 \otimes \mathbf{v}_2 \\ &= \begin{bmatrix} \lambda_1 & 0 & 0 \\ & 1 - \lambda_1 & 0 \\ \text{sym} & & 0 \end{bmatrix} \mathbf{v}_i \otimes \mathbf{v}_j \end{aligned} \quad (9)$$

in the orientation coordinate system $\{\mathbf{v}_i\}$ which is defined in Eq. (6). Positive definiteness and normalization of the trace combined with the ordering convention of the eigenvalues demand the parameter range $1/2 \leq \lambda_1 \leq 1$. Bauer and Böhlke (2021) discuss that planar fiber orientation tensors of fourth order only depend on three independent parameters and derive admissible ranges of these parameters demanding positive semi-definiteness of the orientation tensors. Among the admissible parameters, Bauer and Böhlke (2022) identify a subset of parameter combinations which represent all admissible and structurally distinct planar fourth-order fiber orientation tensors. Following Bauer and Böhlke (2022), two tensors \mathbb{A} and \mathbb{B} are structurally distinct if

$$\exists \mathbf{Q} \in \text{SO}(3) \text{ with } \mathbf{Q} \star \mathbb{A} = \mathbb{B} \quad (10)$$

with the special orthogonal group $\text{SO}(3)$, which contains all proper rotations. These results are summarized by the parameterization in Eq. (11) (see Box I) which follows from Bauer and Böhlke (2022, equation (22)) with

$$\hat{R}(\lambda_1) = (\lambda_1 - \lambda_1^2)/2 \quad (13)$$

and is represented in Kelvin–Mandel notation (Thomson, 1856; Mandel, 1965; Mehrabadi and Cowin, 1990). This notation is explained in detail in Appendix A and the basis $\mathbf{B}_\xi^v \otimes \mathbf{B}_\zeta^v$ is spanned in the orientation coordinate system $\{\mathbf{v}_i\}$, i.e., for example the fifth basis vector in Eq. (11) becomes $\mathbf{B}_5^v = \frac{\sqrt{2}}{2} (\mathbf{v}_1 \otimes \mathbf{v}_3 + \mathbf{v}_3 \otimes \mathbf{v}_1)$. The parameterization in Eq. (11) can be combined with the set of parameter combinations which leads to admissible and distinct $\mathbb{N}^{\text{planar}}$. This set $\hat{\mathcal{N}}^{\text{planar}}$ is given in Eq. (12) following Bauer and Böhlke (2022, equation (28)). A visualization of the body of admissible and distinct orientation tensors $\hat{\mathcal{N}}^{\text{planar}}$ in Cartesian coordinates

$$\hat{d}_1 = \hat{r} \sin(\hat{\beta}), \quad \hat{d}_8 = \hat{r} \cos(\hat{\beta}) \quad (14)$$

$$\mathbb{N}^{\text{planar}}(\lambda_1, \hat{r}, \hat{\beta}) = \left[\begin{array}{ccc|ccc} -\hat{r} \sin(\hat{\beta}) - \hat{R}(\lambda_1) + \lambda_1 & \hat{r} \sin(\hat{\beta}) + \hat{R}(\lambda_1) & 0 & 0 & 0 & \sqrt{2} \hat{r} \cos(\hat{\beta}) \\ & -\hat{r} \sin(\hat{\beta}) - \hat{R}(\lambda_1) + (1 - \lambda_1) & 0 & 0 & 0 & -\sqrt{2} \hat{r} \cos(\hat{\beta}) \\ & & 0 & 0 & 0 & 0 \\ \hline \text{completely} & & & & & \text{symmetric} \end{array} \right] \mathbf{B}_\xi^V \otimes \mathbf{B}_\zeta^V \quad (11)$$

$$\hat{\mathcal{N}}^{\text{planar}} = \left\{ \mathbb{N}^{\text{planar}}(\lambda_1, \hat{r}, \hat{\beta}) \mid \frac{1}{2} < \lambda_1 \leq 1, 0 \leq \hat{r} \leq \hat{R}(\lambda_1), -\frac{\pi}{2} \leq \hat{\beta} \leq \frac{\pi}{2} \right\} \cup \left\{ \mathbb{N}^{\text{planar}}(\lambda_1, \hat{r}, \hat{\beta}) \mid \lambda_1 = \frac{1}{2}, 0 \leq \hat{r} \leq \frac{1}{8}, \hat{\beta} = -\frac{\pi}{2} \right\} \quad (12)$$

Box I.

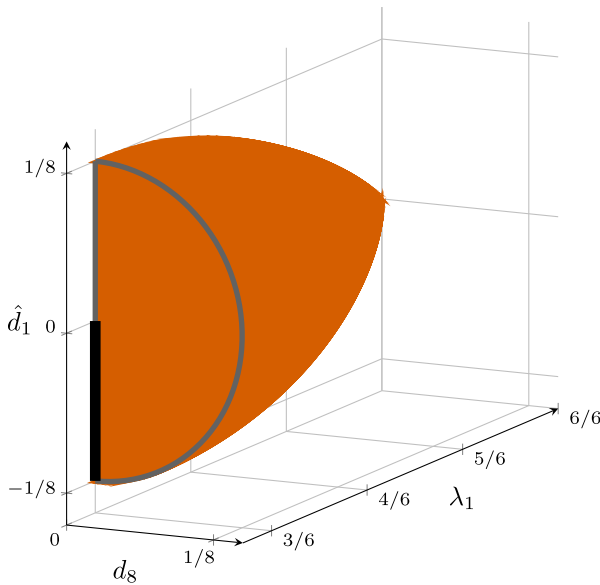


Fig. 2. Visualization of the set of admissible and distinct planar fourth-order fiber orientation tensors $\mathcal{N}^{\text{planar}}$ in the parameter space $\{\lambda_1, \hat{d}_1, \hat{d}_8\}$ using the parameterization of $\mathbb{N}^{\text{planar}}$ in Eq. (11). A derivation of this space is given in Bauer and Böhlke (2022).

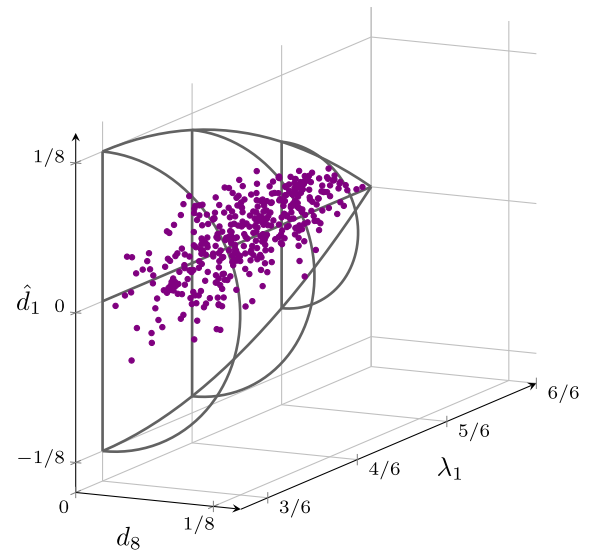


Fig. 3. Fourth-order orientation tensors $\mathcal{N}_{\text{SMC}}^{\text{CT}}$ obtained by computer tomography (CT) scans at several positions of a SMC specimen, represented by points inside the admissible and distinct planar parameter space $\hat{\mathcal{N}}^{\text{planar}}$. The size of the reference volume associated with each discrete fiber orientation tensor significantly determines the resulting distribution inside the admissible region.

is given in Fig. 2. The data set $\mathcal{N}_{\text{SMC}}^{\text{CT}}$ of fiber orientation tensors obtained by CT, which second-order information is visualized in Fig. 1, is represented in the parameter space $\hat{\mathcal{N}}^{\text{planar}}$ in Fig. 3. The data points are preferably concentrated around the axis of vanishing values of \hat{d}_1 and \hat{d}_8 . This observation supports the statement of Hine et al. (2004), that real fiber orientations preferably scatter around orientation states with maximum entropy, i.e., those which are approximately isotropic. Analysis of additional data sets reveals, that the size of the reference volume associated with each discrete fiber orientation tensor significantly determines the resulting distribution inside the admissible region. However, quantitative investigations on the dependence of fiber orientation states on processing and CT settings is moved to a follow-up publication. Based on the parameterization $\mathbb{N}^{\text{planar}}(\lambda_1, \hat{r}, \hat{\beta})$ and the set $\hat{\mathcal{N}}^{\text{planar}}$, a visualization method, motivated by Bauer and Böhlke (2022), can be used to study the influence of planar fourth-order fiber orientation tensors on the mechanical properties predicted by orientation averaging mean field homogenization techniques.

Although, the planar fiber orientation tensors given in Eqs. (9) and (11) fit into a two-dimensional framework, e.g., used in Bauer and Böhlke (2022), a three-dimensional tensor framework is deployed within this work, as the mechanical behavior of real materials is defined by the laws of physics of the three-dimensional world. Boundary condition into the out-of-plane direction influence the mechanical response of planar structures, see Nordmann et al. (2020).

2.3. Orientation averages

Orientation averaging mean field homogenization demands analytical or numerical schemes which yield averages of direction-dependent tensorial quantities over orientations. Advani and Tucker III (1987) define the orientation average of a tensorial quantity \mathbb{A} by

$$\langle \mathbb{A} \rangle_{\text{AT}} = \int_{S^2} \psi(\mathbf{n}) \mathbb{A}(\mathbf{n}) dS, \quad (15)$$

i.e., as a weighted summation with weights defined by the FODF. Several formulations and approximations of Eq. (15) exist in literature. An exact formulation given in the original paper (Advani and Tucker III, 1987, equation (28)), frequently used in, e.g., Lielens et al. (1998), Jack and Smith (2008), Camacho et al. (1990), Brylka (2017), Kehrer et al. (2020), Hessman et al. (2021) is labeled $\langle \cdot \rangle_{\text{ATN}}$ in this work. This formulation is given directly in terms of fiber orientation tensors of second and fourth order Kanatani (1984) first kind, and in its original formulation is restricted to transversely isotropic elasticity tensors $\mathbb{H} = H_{ijkl} \mathbf{e}_i \otimes \mathbf{e}_j \otimes \mathbf{e}_k \otimes \mathbf{e}_l$, i.e., stiffness or compliance-like quantities with major and both minor symmetries which may be specified in index notation by $H_{ijkl} = H_{jikl} = H_{ijlk}$. However, the original formulation in Advani and Tucker III (1987), which is repeated in slightly varying notation in, e.g., Kehrer et al. (2020), Brylka (2017) and Heller

et al., can be extended to transversely isotropic tensors which lack the major symmetry of an elasticity tensor. Such a generalization is given in Appendix D based on the formulation introduced in the next section. The explicit formulation of $\langle \cdot \rangle_{\text{ATN}}$ in orientation tensors is simple and efficient, but complicates adaption of empirical fiber damage (Schemmann et al., 2018b) or incorporation of direction-dependent fiber length distributions (Brylka, 2017). A reformulation based on the harmonic decomposition (Rychlewski, 2000; Forte and Vianello, 1996; Olive et al., 2018; Böhlke and Brüggemann, 2001) explicitly revealing the structure of the scheme is given in the next section.

2.3.1. Reformulation of the explicit Advani–Tucker orientation average

A transversely isotropic elasticity tensor is completely defined by five independent parameters and a direction, i.e., a normal vector \mathbf{q} , and can be written as $\mathbb{C}^{\text{transv}}(h_1, h_2, h_3, h_4, h_5, \mathbf{q})$ following Eq. (B.3) in Appendix B. The orientation average $\langle \cdot \rangle_{\text{ATN}}$ of a transversely isotropic elasticity tensor is independent of \mathbf{q} and given by

$$\begin{aligned} & \langle \mathbb{C}^{\text{transv}}(h_1, h_2, h_3, h_4, h_5, \mathbf{q}) \rangle_{\text{ATN}}(\mathbb{N}) \\ &= h_1 \mathbb{P}_1 + h_2 \mathbb{P}_2 \\ &+ h_3 \mathbb{J}_3 [\text{dev}(\mathbb{N})] + h_4 \mathbb{J}_4 [\text{dev}(\mathbb{N})] + h_5 \text{dev}(\mathbb{N}) \end{aligned} \quad (16)$$

with the irreducible parts of \mathbb{N}

$$\text{dev}(\mathbb{N}) = \mathbb{N} - \mathbb{N}^{\text{iso}} \quad (17)$$

$$\text{dev}(\mathbb{N}) = \mathbb{N} - \frac{6}{7} \text{sym}(\text{dev}(\mathbb{N}) \otimes \mathbf{I}) - \mathbb{N}^{\text{iso}} \quad (18)$$

and the isotropic parts of the second- and fourth-order fiber orientation tensors of Kanatani (1984) first kind

$$\mathbb{N}^{\text{iso}} = \frac{1}{3} \mathbf{I}, \quad \mathbb{N}^{\text{iso}} = \frac{7}{35} \text{sym}(\mathbf{I} \otimes \mathbf{I}) \quad (19)$$

following Bauer and Böhlke (2021). The isotropic sixth order tensors \mathbb{J}_3 and \mathbb{J}_4 are defined in Eqs. (B.6) and (B.7). The operator $\text{sym}(\cdot)$ extracts the totally symmetric part following Spencer (1970) and the operator $\text{dev}(\cdot)$ extracts the deviatoric part also discussed in Spencer (1970). Linearity of the harmonic decomposition in Eq. (16) implies that the orientation average following Advani and Tucker III (1987) is linear in both $\mathbb{C}^{\text{transv}}$ and \mathbb{N} . This implication might be obvious to some authors, as the only source of orientation dependent structural information is \mathbb{N} . However, the original formulation in Advani and Tucker III (1987) does not directly reveal, that the isotropic part of the averaged elasticity tensor is unaffected, as one would expect from a physical point of view. In addition, the first and second deviatoric parts of the orientation average in Eq. (16), i.e., $h_3 \text{dev}(\mathbb{N})$ and $h_4 \text{dev}(\mathbb{N})$, only differ by a scaling factor and share the tensor structure of $\text{dev}(\mathbb{N})$. As \mathbb{N} is completely symmetric, its first and second deviatoric parts coincide, see Bauer and Böhlke (2021). As the manual derivation of Eq. (16) is lengthy, listing 1 combined with code in Bauer (2022) is used to validate the representation of the orientation average. Any material model which contains the Advani–Tucker orientation average, implicitly contains a linearity assumption of at least an intermediate quantity in the fiber orientation or fabric tensor. For reference, some authors (Schemmann et al., 2018a,b; Karl et al., 2021) explicitly postulate linearity of an effective stiffness or viscosity in fiber orientation or fabric tensors. In contrast, a material model of a porous, anisotropic, linear elastic material being non-linear in a fabric tensor is given in Cowin (1985).

2.3.2. Direct numerical integration and the adaptive scheme based on angular central Gaussian distributions

Direct numerical integration of Eq. (15) requires both a given FODF and a large number of integration points on the two-dimensional area of integration S^2 , but leads to insufficient accuracy despite high numerical effort, especially in the case of strongly localized FODF. This performance and accuracy issue motivates a recently developed numerical scheme (Goldberg et al., 2017) denoted by $\langle \cdot \rangle_{\text{ATGOS}}$ which is based on a special class of FODF basis functions called angular central

Gaussian. Although, this scheme is not used within this work, it is shortly introduced as a comparison. The scheme $\langle \cdot \rangle_{\text{ATGOS}}$ leads to an approximation resulting in a weighted summation of the quantity of interest pointing into a number of N^{GOS} discrete directions

$$\langle \mathbb{A} \rangle_{\text{AT}} \approx \langle \mathbb{A} \rangle_{\text{ATGOS}}(\mathbb{N}) = \sum_i^{N^{\text{GOS}}} w_i^{\text{GOS}}(\mathbb{N}) \mathbb{A}(\mathbf{n}_i) \quad (20)$$

with the weights being a function of the second-order fiber orientation tensor. The weights can be pre-calculated and stored in efficient look-up structures. Implementation details are given for the three-dimensional case in Goldberg et al. (2017) and Hessman et al. (2021) and for the two-dimensional case in Görthofer et al. (2020). This formulation yields reasonable accuracy even for localized FODF with a limited number of integration points (Goldberg et al., 2017), e.g., $N^{\text{GOS}} = 434$ in Hessman et al. (2021). Due to the structure in Eq. (20), any direction-dependent quantity can be averaged and the weights may be modeled for empirical simulation of damage. However, the orientation average $\langle \cdot \rangle_{\text{ATGOS}}$ is solely based on the directional information contained within a second-order orientation tensor, which is limited to two scalars describing the half axes of an ellipsoid combined with the definition of a coordinate system.

2.3.3. Orientation average by reconstructed planar FODF based on a maximum entropy method

A maximum entropy FODF reconstruction for planar fiber orientations developed by Bauer and Böhlke (2022) based on Müller and Böhlke (2016), can be combined with any numerical integration on S^1 leading to an approximation of the Advani–Tucker orientation average, which shares the simple structure of $\langle \mathbb{A} \rangle_{\text{ATGOS}}$, uses fourth-order fiber orientation tensor information and makes use of the reduced dimension of planar fiber orientation tensors. However, as this scheme uses direct numerical integration on S^1 , it leads to insufficient accuracy for localized fiber orientation states. Fortunately, the localized orientation states are known through analysis of the admissible region $\mathcal{N}^{\text{planar}}$ in Bauer and Böhlke (2022) and can be captured in implementations. Following Bauer and Böhlke (2022), for any admissible non-localized fiber orientation tensor of fourth-order, a planar FODF, $\hat{\psi}^{\text{ME}}(\varphi, \mathbb{N}^{\text{planar}})$ parameterized in one spherical angle defined in Eq. (8) with $0 \leq \varphi < 2\pi$ can be identified. This leads to an approximation of the Advani–Tucker average in Eq. (15) for the planar case by

$$\begin{aligned} \langle \mathbb{A} \rangle_{\text{AT}}(\mathbb{N}^{\text{planar}}) &\approx \langle \mathbb{A} \rangle_{\text{ME}}(\mathbb{N}^{\text{planar}}) \\ &= \int_0^{2\pi} \hat{\psi}^{\text{ME}}(\varphi, \mathbb{N}^{\text{planar}}) \mathbf{Q}(\varphi) \star \mathbb{A} \, d\varphi \\ &\approx 2\pi \sum_{i=1}^{N^{\text{ME}}} w_i \hat{\psi}^{\text{ME}}(\varphi_i, \mathbb{N}^{\text{planar}}) \mathbf{Q}(\varphi_i) \star \mathbb{A} \\ &= 2\pi \sum_{i=1}^{N^{\text{ME}}} w_i^{\text{ME}}(\mathbb{N}^{\text{planar}}) \mathbf{Q}(\varphi_i) \star \mathbb{A} \end{aligned} \quad (21)$$

with a rotation around the \mathbf{v}_3 axis \mathbf{Q} , evaluated at specified angles which are defined by any numerical integration scheme on S^1 with weights w_i . Within this work, numerical integration on S^1 with homogeneous weights $w_i = 1/N^{\text{ME}}$ and equidistant angles $w_i = 2\pi i/N^{\text{ME}}$ following Krylov and Stroud (2006) is used. The weights of the numerical integration scheme might be combined with the direction specific value of the FODF in Eq. (21). The accuracy of the average $\langle \cdot \rangle_{\text{ME}}$ is assessed by averaging of moment tensors, as

$$\langle \mathbf{n}^{\otimes 4} \rangle_{\text{AT}}(\mathbb{N}^{\text{planar}}) = \mathbb{N}^{\text{planar}} \approx \langle \mathbf{n}^{\otimes 4} \rangle_{\text{ME}}(\mathbb{N}^{\text{planar}}) \quad (22)$$

has to hold. The assessment is done for all fourth-order fiber orientation tensors specified in Table G.2 except for the unidirectional case notated as $\mathcal{N}_{\text{selected}}^{\text{planar}}$, as this localized orientation state is insufficiently handled by the numerical integration. The deviation is quantified by

$$\Delta^{\max}(N^{\text{ME}}) = \max_{\mathbb{N} \in \mathcal{N}_{\text{selected}}^{\text{planar}}} \frac{\| \langle \mathbf{n}^{\otimes 4} \rangle_{\text{ME}}(N^{\text{ME}}, \mathbb{N}) - \mathbb{N} \|}{\| \mathbb{N} \|} \quad (23)$$

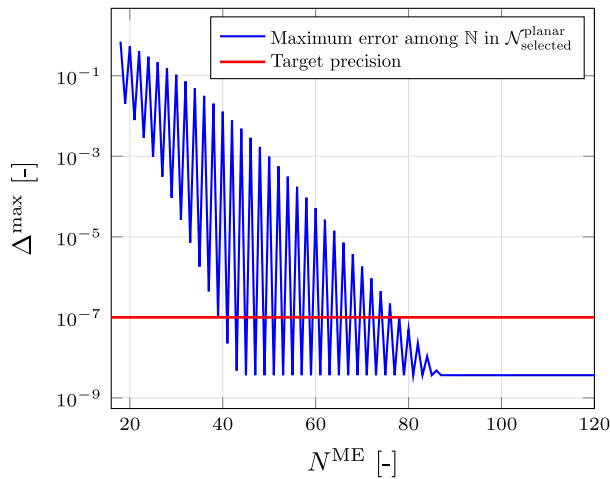


Fig. 4. Influence of the number of integration points on the deviation of $\langle \mathbf{n}^{\otimes 4} \rangle_{\text{ME}}$ from $\langle \mathbf{n}^{\otimes 4} \rangle_{\text{ATN}}$ with Δ^{max} defined in Eq. (23).

and given for varying order of the numerical integration N^{ME} in Fig. 4. The target precision of 10^{-7} is reached. Studying the convergence of the numerical averaging scheme by averaging a specific, randomly chosen, elasticity tensor instead of the moment tensor in Eq. (23), following Hessman et al. (2021), leads to similar convergence.

2.4. Orientation averaging mean field homogenization

Sheet molding compound is a two-phase composite with glass fibers embedded irregularly in a thermoset polymer matrix. For isothermal applications, isotropic linear elasticity states a reasonable assumption for both the fiber and the matrix behavior, see Kehrer et al. (2020). In consequence, the local stress–strain relation inside the fiber and matrix phase at position \mathbf{x} is

$$\boldsymbol{\sigma}(\mathbf{x}) = \mathbb{C}_f [\boldsymbol{\varepsilon}(\mathbf{x})] \quad \forall \mathbf{x} \in \mathcal{B}_f \quad (24)$$

$$\boldsymbol{\sigma}(\mathbf{x}) = \mathbb{C}_m [\boldsymbol{\varepsilon}(\mathbf{x})] \quad \forall \mathbf{x} \in \mathcal{B}_m \quad (25)$$

with parts of the representative volume element (RVE) occupied by the fibers \mathcal{B}_f and the matrix \mathcal{B}_m , respectively. The stiffness of a fiber is denoted by \mathbb{C}_f and \mathbb{C}_m represents the stiffness of the matrix. Isotropy implies that \mathbb{C}_f and \mathbb{C}_m in Eqs. (24) and (25) do not depend on the spatial orientation and are given by

$$\mathbb{C}_f = 3K_f \mathbb{P}_1 + 2G_f \mathbb{P}_2 \quad (26)$$

$$\mathbb{C}_m = 3K_m \mathbb{P}_1 + 2G_m \mathbb{P}_2 \quad (27)$$

with the first and second isotropic projectors \mathbb{P}_1 and \mathbb{P}_2 respectively and bulk and shear modulus denoted by K and G . Throughout this work, material parameters are adopted from Kehrer et al. (2020, Table 2) and listed in Table 1. Two one-point characteristics describing the microstructure of a RVE at a material point inside a SMC-component are considered. The first characteristic is the volume fraction of the fibers c_f , which implies the volume fraction of the matrix $c_m = 1 - c_f$. The second characteristic is a fourth-order fiber orientation tensor \mathbb{N} . In the absence of any non-linearities, such as cracks, the effective elastic stiffness $\hat{\mathbb{C}}$ of the RVE exists and is of interest. The effective stiffness maps effective strains $\bar{\boldsymbol{\varepsilon}} = \langle \boldsymbol{\varepsilon}(\mathbf{x}) \rangle$ onto effective stresses $\bar{\boldsymbol{\sigma}} = \langle \boldsymbol{\sigma}(\mathbf{x}) \rangle$ by $\bar{\boldsymbol{\sigma}} = \hat{\mathbb{C}}[\bar{\boldsymbol{\varepsilon}}]$. (28)

The operator $\langle \cdot \rangle$ takes the volume average of a spatially varying field quantity, e.g., $\boldsymbol{\sigma}(\mathbf{x})$, inside the RVE. Four mean field approximations are briefly reviewed and examined for given material parameters and variable fiber orientation tensors.

Table 1

Material parameters of the SMC constituents glass fiber and neat matrix (UPPH, i.e., unsaturated polyester–polyurethane hybrid) adopted from Kehrer et al. (2020, Table 2) citing additional references. Bulk and shear modulus are derived from Young's modulus and Poisson's ratio. The volume fractions of the fiber and matrix phases are $c_p = 0.256$ and $c_p = 0.744$.

	Young's modulus	Poisson's ratio	Bulk modulus	Shear modulus
Fibers	73.0 GPa	0.22	43.45 GPa	29.92 GPa
Matrix	3.4 GPa	0.385	4.93 GPa	1.23 GPa

2.4.1. Two-step Hashin–Shtrikman

A two-step Hashin–Shtrikman scheme for fiber reinforced composites following Kehrer et al. (2020), based on Walpole (1966a,b, 1969) and proposed by Fernández and Böhlke (2019) is used to study the influence of a fourth-order orientation tensor on the effective stiffness. Detailed derivations of the Hashin–Shtrikman bounds, based on a variational principle, are given in Walpole (1966a) and Fernández and Böhlke (2019). In this work only the resulting equations are of interest. Under the assumption of phase-wise constant stress polarizations, the Green's function of a material without long-range order and ellipsoidal two-point statistics, is constant (Fernández and Böhlke, 2019, section 2.2). This constant Green's function is represented by the Hill's (Hill, 1965) polarization tensor \mathbb{P} and reflects the ellipsoidal symmetry of the two-point statistics. Under these assumptions, the effective stiffness of a material made up of n phases with stiffnesses $\{\mathbb{C}_i\}$ for $i \in [1, \dots, n]$ is given as a function of a comparison stiffness \mathbb{C}_0 by

$$\begin{aligned} \hat{\mathbb{C}}^{\text{HSW}}(\mathbb{C}_0, \mathbb{P}(\mathbb{C}_0, a), \{\mathbb{C}_i\}, \langle \langle \cdot \rangle \rangle) \\ = \mathbb{C}_0 - \mathbb{P}^{-1} + [\langle \langle \mathbb{W}(\mathbb{C}_0, \mathbb{P}, \mathbb{C}_i) \rangle \rangle]^{-1} \end{aligned} \quad (29)$$

with

$$\mathbb{W}(\mathbb{C}_0, \mathbb{P}, \mathbb{C}_i) = [\mathbb{P}^{-1} + \mathbb{C}_i - \mathbb{C}_0]^{-1} \quad (30)$$

and with $\mathbb{P}(\mathbb{C}_0, a)$ depending on the symmetry of the two point statistics. For simplicity, the dependence of \mathbb{P} upon the two point statistic is represented by an aspect ratio a with $1/2 \leq a \leq \infty$ reaching from the isotropic case $\mathbb{P}^0(\mathbb{C}_0) = \mathbb{P}(\mathbb{C}_0, 1/2)$ to the limiting unidirectional case $\mathbb{P}^{\text{UD}}(\mathbb{C}_0) = \mathbb{P}(\mathbb{C}_0, \infty)$. This restriction of \mathbb{P} from generally ellipsoidal shapes to spheroidal shapes is common in the context of fiber reinforced composites. The operator $\langle \langle \cdot \rangle \rangle$ takes the average over the RVE. Alternative formulations of the Hashin–Shtrikman scheme exist, e.g., in Willis (1977, 1981) and remarks on the different formulations are given in Fernández and Böhlke (2019). The formulation in Eq. (29) is not directly applicable to singular, i.e., non-invertible, polarization tensors. However, Walpole (1969, page 238) proposes a dual scheme which can be used to evaluate Eq. (29) for singular polarization tensors, e.g., \mathbb{P}^{UD} . If the comparison material with stiffness \mathbb{C}_0 is selected, such that the stiffnesses of all phases are smaller (larger) than \mathbb{C}_0 , e.g., using first order bounds, Eq. (29) yields a lower (upper) Hashin–Shtrikman bound. As SMC is a two-phase composite, for any choice of the comparison stiffness \mathbb{C}_0 in between \mathbb{C}_m and \mathbb{C}_f , Eq. (29) gives an admissible effective stiffness in between the Hashin–Shtrikman bounds. Following Kehrer et al. (2020, equation (24)), a comparison stiffness as a function of an interpolation parameter k is introduced by

$$\hat{\mathbb{C}}_0(k) = [1 - k] \mathbb{C}_m + k \mathbb{C}_f \quad (31)$$

with $0 \leq k \leq 1$. With this notation, the scheme of Kehrer et al. (2020) is reformulated as a generic two-step Hashin–Shtrikman scheme. In a first step, the effective stiffness of an artificially pseudo grain $\hat{\mathbb{C}}^{\text{UD}}$ is calculated by

$$\begin{aligned} \hat{\mathbb{C}}^{\text{UD}}(k_1, c_f, \mathbb{C}_f, \mathbb{C}_m) = \hat{\mathbb{C}}^{\text{HSW}}\left(\mathbb{C}_0 = \hat{\mathbb{C}}_0(k_1), \mathbb{P} = \mathbb{P}^{\text{UD}}(\mathbb{C}_0), \right. \\ \left. \{\mathbb{C}_i\} = \{\mathbb{C}_f, \mathbb{C}_m\}, \langle \langle \cdot \rangle \rangle = \langle \cdot \rangle(c_f)\right). \end{aligned} \quad (32)$$

This pseudo grain contains unidirectional fibers with a volume content which is equal to the volume content of the fibers in the overall two-phase composite c_f . To be explicit, the operator $\langle \cdot \rangle$ in Eq. (32) applied to $\mathbb{W}(C_0, \mathbb{P}, C_i)$ with $i \in [m, f]$ reads as $\langle \mathbb{W}(\dots, C_i) \rangle = c_m \mathbb{W}(\dots, C_m) + c_f \mathbb{W}(\dots, C_f)$, with the abbreviation “...” for additional function arguments. The stiffness $\bar{\mathbb{C}}^{\text{UD}}$ obtained by Eq. (32) is transversely isotropic. As the Hill polarization \mathbb{P} in Eqs. (30) and (32) reflects the shape of the two-point statistics, the specific choice of \mathbb{P}^{UD} for a single grain implies a laminate-like two-point statistic. It should be noted, that the inclusion shape is not specified. However, specification of the two-point statistic is not independent of the inclusion shape. In the second step, the stiffness obtained in step one is orientation averaged based on the Hashin–Shtrikman scheme in Eq. (29), where the average over the RVE $\langle \langle \cdot \rangle \rangle$ is transferred into an average over orientations. The operator $\langle \cdot \rangle_{\text{ATN}}$ defined in Eq. (16) represents a commonly used (Lielens et al., 1998; Jack and Smith, 2008; Camacho et al., 1990) average over orientations, based on a fourth-order fiber orientation tensor \mathbb{N} , following Advani and Tucker III (1987). As the pseudo grain is artificial, the two-point statistics in the second step are assumed to be isotropic and are therefore reflected by the Hill polarization tensor for spherical inclusions \mathbb{P}^0 . This leads to the approximation $\bar{\mathbb{C}}^{\text{HSW}2}$ of the effective overall stiffness with

$$\bar{\mathbb{C}}^{\text{HSW}2}(k_1, k_2, \mathbb{N}, c_f, C_f, C_m) = \bar{\mathbb{C}}^{\text{HSW}}(C_0 = \hat{C}_0(k_2), \mathbb{P} = \mathbb{P}^0(C_0), \{C_i\} = \{\bar{\mathbb{C}}^{\text{UD}}(k_1, \dots)\}, \langle \langle \cdot \rangle \rangle = \langle \cdot \rangle_{\text{ATN}}(\mathbb{N})). \quad (33)$$

The connection to the formulas in Kehrner et al. (2020) is given in Appendix E. The formulation of $\langle \cdot \rangle_{\text{ATN}}$ in Eq. (16) shows the linearity of the orientation average in both arguments.

For the special case of planar fourth-order orientation information, i.e., $\mathbb{N}^{\text{planar}}$ and a given transversely isotropic pseudo grain stiffness $\bar{\mathbb{C}}^{\text{UD}}$, the structure of the effective stiffness is given analytically. Starting from a given transversely isotropic stiffness $\bar{\mathbb{C}}^{\text{UD}}$ obtained in a first homogenization step, e.g., following Eq. (32), the second homogenization step in Eq. (33) for the special case of a planar orientation tensor $\mathbb{N}^{\text{planar}}$, is of interest. Omitting functional dependencies, the expansion of Eq. (29) reads as

$$\bar{\mathbb{C}}^{\text{HSW}} = C_0 - [\mathbb{P}^0]^{-1} + \mathbb{G} \quad (34)$$

with

$$\mathbb{G} = [\langle [[\mathbb{P}^0]^{-1} + \bar{\mathbb{C}}^{\text{UD}} - C_0]_{\text{ATN}} \rangle^{-1}]^{-1} = [\langle \mathbb{A}^{-1} \rangle_{\text{ATN}}]^{-1} = [\langle \mathbb{B} \rangle_{\text{ATN}}]^{-1} = [\mathbb{E}]^{-1}. \quad (35)$$

The Hill polarization \mathbb{P}^0 is isotropic and its inverse is given by

$$[\mathbb{P}^0]^{-1} = h_1^{\text{P}0} \mathbb{P}_1 + h_2^{\text{P}0} \mathbb{P}_2 \quad (36)$$

with

$$h_1^{\text{P}0} = h_1^0 + 2h_2^0, \quad h_2^{\text{P}0} = \frac{\frac{5}{2}h_2^0 [h_1^0 + 2h_2^0]}{h_1^0 + 3h_2^0} \quad (37)$$

and $h_1^0 = 3K^0$, $h_2^0 = 2G^0$ and the bulk and shear modulus of the isotropic comparison material K^0 and G^0 . As both the Hill polarization and the stiffness of the comparison material are isotropic, the intermediate quantity \mathbb{A} in Eq. (35) inherits the transversely isotropic symmetry from the unidirectional stiffness $\bar{\mathbb{C}}^{\text{UD}}$. With the short hand notation of a transversely isotropic elasticity tensor defined in Eq. (B.13) the tensor \mathbb{A} is given by

$$\mathbb{A} = [h_1, h_2, h_3, h_4, h_5, \mathbf{q} = \mathbf{v}_1] \quad (38)$$

with

$$h_1 = h_1^{\text{P}0} - h_1^0 + h_1^{\text{UD}}, \quad h_2 = h_2^{\text{P}0} - h_2^0 + h_2^{\text{UD}}, \quad (39)$$

$$h_3 = h_3^{\text{UD}}, \quad h_4 = h_4^{\text{UD}}, \quad h_5 = h_5^{\text{UD}} \quad (40)$$

based on

$$\bar{\mathbb{C}}^{\text{UD}} = [h_1^{\text{UD}}, h_2^{\text{UD}}, h_3^{\text{UD}}, h_4^{\text{UD}}, h_5^{\text{UD}}, \mathbf{q} = \mathbf{v}_1]. \quad (41)$$

As the orientation of the pseudo grain stiffness is arbitrary, without loss of generality, $\mathbf{q} = \mathbf{v}_1$ holds in Eqs. (38) and (41). The inversion of a transversely isotropic stiffness is discussed in, e.g., (Lubarda and Chen, 2008, Eq. (31)), and leads to a transversely isotropic compliance

$$\mathbb{B} = \mathbb{A}^{-1} = [h_1^{\text{B}}, h_2^{\text{B}}, h_3^{\text{B}}, h_4^{\text{B}}, h_5^{\text{B}}, \mathbf{q} = \mathbf{v}_1] \quad (42)$$

$$= \begin{bmatrix} B_{11} & B_{12} & B_{12} & 0 & 0 & 0 \\ & B_{22} & B_{23} & 0 & 0 & 0 \\ & & B_{22} & 0 & 0 & 0 \\ & & & B_{22} - B_{23} & 0 & 0 \\ \text{sym} & & & & 2B_{55} & 0 \\ & & & & & 2B_{55} \end{bmatrix} \mathbf{B}_\xi \otimes \mathbf{B}_\zeta$$

with h_i^{B} for $i \in \{1, 2, 3, 4, 5\}$ given in Appendix F in Eqs. (F.1) to (F.7). The general correspondence of stiffness and compliance is discussed in Rychlewski (1984). Simpler representations of a transversely isotropic compliance (Lubarda and Chen, 2008; Cowin and Van Buskirk, 1986; Vannucci, 2018), e.g., in tensor components or engineering notation, exist. However, Eqs. (F.1) to (F.7) show the interaction of the harmonic coefficients h_i with $i \in \{1, 2, 3, 4, 5\}$ during the tensor inversion. Each coefficient of \mathbb{B} is a function of all five coefficients of \mathbb{A} . Taking the orientation average (Advani and Tucker III, 1987) of \mathbb{B} , e.g., using Eq. (16), leads to

$$\mathbb{E} = \langle \mathbb{B} \rangle_{\text{ATN}} \quad (43)$$

$$= \begin{bmatrix} E_{11} & E_{12} & E_{13} & 0 & 0 & E_{16} \\ & E_{22} & E_{23} & 0 & 0 & -E_{16} \\ & & E_{33} & 0 & 0 & 0 \\ & & & E_{44} & 0 & 0 \\ \text{sym} & & & & E_{55} & 0 \\ & & & & & E_{66} \end{bmatrix} \mathbf{B}_\xi \otimes \mathbf{B}_\zeta.$$

The tensor components in Eq. (43) are specified in Eqs. (F.8) to (F.17) in Appendix F. The inversion of \mathbb{E} leads to

$$\mathbb{G} = [\mathbb{E}]^{-1} \quad (44)$$

$$= \begin{bmatrix} G_{11} & G_{12} & G_{13} & 0 & 0 & G_{16} \\ & G_{22} & G_{23} & 0 & 0 & G_{26} \\ & & G_{33} & 0 & 0 & G_{36} \\ & & & G_{44} & 0 & 0 \\ \text{sym} & & & & G_{55} & 0 \\ & & & & & G_{66} \end{bmatrix} \mathbf{B}_\xi \otimes \mathbf{B}_\zeta$$

with tensor components given in Eqs. (F.18) to (F.31) in Appendix F. Eqs. (F.18) to (F.31) combined with Eqs. (F.8) to (F.17) show that the effective stiffness $\bar{\mathbb{C}}^{\text{HSW}}$ is nonlinear in the parameters of the fiber orientation tensor λ_1, d_1, d_8 . In addition, the structure of $\bar{\mathbb{C}}^{\text{HSW}}$ and \mathbb{G} differs from that of the intermediate quantity \mathbb{E} , as the tensor component G_{36} in Eq. (44) does not vanish, although E_{36} in Eq. (43) does vanish. $\bar{\mathbb{C}}^{\text{HSW}}$ inherits the structure from \mathbb{G} .

2.4.2. Orientation averaging Mori–Tanaka following (Benveniste, 1987)

Various aspects of the orientation averaging Mori–Tanaka approximation are discussed in Brylka (2017), Weng (1990) and Qiu and Weng (1990). Nevertheless, a comprehensive summary of the basic equations for the special case of homogeneous fiber lengths, i.e., an isotropic fiber length distribution, is given hereafter. The RVE is denoted by B and any point inside the RVE is identifiable by a position $\mathbf{x} \in B$. Introducing a field of strain localization tensors $\mathbb{A}(\mathbf{x})$ mapping the effective strain of the RVE, $\bar{\boldsymbol{\varepsilon}}$, onto the local strain $\boldsymbol{\varepsilon}(\mathbf{x})$ with

$$\boldsymbol{\varepsilon}(\mathbf{x}) = \mathbb{A}(\mathbf{x})[\bar{\boldsymbol{\varepsilon}}] \quad (45)$$

yields an exact representation of the effective stiffness by

$$\bar{\mathbb{C}} = \langle \mathbb{C}(\mathbf{x})\mathbb{A}(\mathbf{x}) \rangle \quad (46)$$

due to

$$\bar{\sigma} = \langle \sigma(\mathbf{x}) \rangle = \langle \mathbb{C}(\mathbf{x})[\varepsilon(\mathbf{x})] \rangle = \langle \mathbb{C}(\mathbf{x})\mathbb{A}(\mathbf{x})[\bar{\varepsilon}] \rangle = \langle \mathbb{C}(\mathbf{x})\mathbb{A}(\mathbf{x}) \rangle [\bar{\varepsilon}]. \quad (47)$$

If the exact strain localization field $\mathbb{A}(\mathbf{x})$ for an RVE is known, the effective stiffness $\bar{\mathbb{C}}$ is given by Eq. (46). The volume average of Eq. (46) implies $\langle \mathbb{A}(\mathbf{x}) \rangle = \mathbb{I}^s$ with \mathbb{I}^s being the identity acting on the space of symmetric second-order tensors. An exact decomposition of the volume average over the RVE into volume averages over the different phases in the special case of a two phase composite yields

$$\langle \mathbb{A} \rangle = \mathbb{I}^s = c_m \langle \mathbb{A} \rangle_m + c_f \langle \mathbb{A} \rangle_f \quad (48)$$

with the volume fraction c_α of phase $\alpha \in \{f, m\}$ and therefore

$$\langle \mathbb{A} \rangle_m = \frac{1}{c_m} [\mathbb{I}^s - c_f \langle \mathbb{A} \rangle_f]. \quad (49)$$

For a two-phase material with piece-wise constant stiffnesses, Eq. (46) combined with Eq. (49) leads to

$$\bar{\mathbb{C}} = c_m \langle \mathbb{C}(\mathbf{x})\mathbb{A}(\mathbf{x}) \rangle_m + c_f \langle \mathbb{C}(\mathbf{x})\mathbb{A}(\mathbf{x}) \rangle_f \quad (50)$$

$$= c_m \mathbb{C}_m \langle \mathbb{A}(\mathbf{x}) \rangle_m + c_f \mathbb{C}_f \langle \mathbb{A}(\mathbf{x}) \rangle_f \quad (51)$$

$$= c_m \mathbb{C}_m \frac{1}{c_m} [\mathbb{I}^s - c_f \langle \mathbb{A} \rangle_f] + c_f \mathbb{C}_f \langle \mathbb{A}(\mathbf{x}) \rangle_f \quad (52)$$

$$= \mathbb{C}_m + c_f \Delta \mathbb{C} \langle \mathbb{A} \rangle_f \quad (53)$$

introducing the short hand notation for the material contrast $\Delta \mathbb{C} = \mathbb{C}_f - \mathbb{C}_m$. The strain localization tensor of the Mori–Tanaka approximation (Mori and Tanaka, 1973) for a two-phase composite reads as

$$\langle \mathbb{A} \rangle_f \approx \langle \mathbb{A} \rangle_f^{\text{MT}} = \mathbb{A}_f^{\text{SI}} [c_m \mathbb{I}^s + c_f \mathbb{A}_f^{\text{SI}}]^{-1} = [c_m [\mathbb{A}_f^{\text{SI}}]^{-1} + c_f \mathbb{I}^s]^{-1} \quad (54)$$

with the strain localization tensor of the inclusion (fiber) phase in the single inclusion problem \mathbb{A}_f^{SI} (Eshelby, 1957) given by

$$\mathbb{A}_f^{\text{SI}} = [\mathbb{P}(\mathbb{C}_m, a) [\mathbb{C}_f - \mathbb{C}_m] + \mathbb{I}^s]^{-1}. \quad (55)$$

The Hill polarization tensor $\mathbb{P}(\mathbb{C}_m, a)$ for spheroidal inclusion shapes is parameterized by an aspect ratio a . Inserting the approximated strain localization tensor of Eq. (54) into Eq. (53) leads to the effective stiffness of the Mori–Tanaka approximation for a two-phase composite

$$\bar{\mathbb{C}}^{\text{MT}}(c_f, \mathbb{C}_f, \mathbb{C}_m, \mathbb{P}) = \mathbb{C}_m + c_f \Delta \mathbb{C} \langle \mathbb{A} \rangle_f^{\text{MT}}. \quad (56)$$

The Hill polarization \mathbb{P} in the single inclusion problem reflects the shape of the inclusion. A study on the influence of the inclusion shape onto the effective stiffness is given in Müller (2016). The large aspect ratio of SMC fibers motivates the use of \mathbb{P}^{UD} , e.g., in Kehrer et al. (2020). Orientation averaging Mori–Tanaka for two-phase composites with anisotropic constituents and an inclusion phase consisting of aligned or randomly orientated ellipsoidal particles following Benveniste (1987) combined with an orientation averaging scheme following Advani and Tucker III (1987), depicted by $\langle \cdot \rangle_{\text{ATN}}$, reads as

$$\langle \mathbb{A} \rangle_f \approx \langle \mathbb{A} \rangle_f^{\text{MTOAB}}(\mathbb{N}, c_f, \mathbb{C}_f, \mathbb{C}_m) \quad (57)$$

$$= [c_m [[\Delta \mathbb{C}]^{-1} \langle \Delta \mathbb{C} \mathbb{A}_f^{\text{SI}} \rangle_{\text{ATN}}(\mathbb{N})]^{-1} + c_f \mathbb{I}^s]^{-1}$$

leading to the Mori–Tanaka orientation averaging approximation following Benveniste (1987) with

$$\bar{\mathbb{C}}^{\text{MTOAB}}(\mathbb{N}, c_f, \mathbb{C}_f, \mathbb{C}_m) = \mathbb{C}_m + c_f \Delta \mathbb{C} \langle \mathbb{A} \rangle_f^{\text{MTOAB}}(\mathbb{N}, c_f, \mathbb{C}_f, \mathbb{C}_m). \quad (58)$$

Orientation averaging Mori–Tanaka following Benveniste (1987) is used in Brylka (2017) and Schemmann et al. (2018b) and limitations are discussed in, e.g., (Benveniste et al., 1991). As the orientation averaging scheme $\langle \cdot \rangle_{\text{ATN}}$ in its original formulation is limited to elasticity tensors, i.e., any tensor $\mathbb{C} = C_{ijkl} \mathbf{e}_i \otimes \mathbf{e}_j \otimes \mathbf{e}_k \otimes \mathbf{e}_l$ with both minor and the major symmetries $C_{ijkl} = C_{jikl} = C_{ijlk} = C_{klij}$, but strain localization tensors may lack the main symmetry, an intermediate elasticity tensor $\Delta \mathbb{C} \mathbb{A}_f^{\text{SI}} = [\mathbb{P} + \Delta \mathbb{C}^{-1}]^{-1}$ is averaged in Eq. (57) before the effect of $\Delta \mathbb{C}$ is removed by $\Delta \mathbb{C}^{-1}$. This step could be avoided using the generalization of the orientation average $\langle \cdot \rangle_{\text{ATN}}$ in Appendix D. The unity of all fibers is treated as one phase.

2.4.3. Direct orientation average of a transversely isotropic stiffness

Some authors (Iorga et al., 2008; Schjødt-Thomsen and Pyrz, 2001) identify the linear orientation average (Advani and Tucker III, 1987) of transversely isotropic stiffness as an approximation for the effective stiffness with

$$\bar{\mathbb{C}}^{\text{MTLinearStiffness}}(\mathbb{N}, \dots) = \langle \bar{\mathbb{C}}^{\text{MT}}(\dots) \rangle_{\text{ATN}}(\mathbb{N}) \quad (59)$$

which is based on the Mori–Tanaka approximation in Eq. (56) and is used in commercial software (Smith, 2019).

2.4.4. Direct orientation average of a transversely isotropic compliance

In analogy to the approximation defined in Eq. (59), another approximation is given by the orientation average of an unidirectional compliance obtained by the Mori–Tanaka approximation

$$\bar{\mathbb{C}}^{\text{MTLinearCompliance}}(\mathbb{N}, \dots) = [\langle [\bar{\mathbb{C}}^{\text{MT}}(\dots)]^{-1} \rangle_{\text{ATN}}(\mathbb{N})]^{-1}. \quad (60)$$

2.5. Graphical representation of elasticity tensors

The last building block for the systematic investigation of the dependence of linear elastic effective stiffness tensors on planar fiber orientation tensors, is a compact, preferably two-dimensional, visualization of effective stiffness tensors. Following Böhlke and Brüggemann (2001), two scalar functions $E(\mathbb{C}, \mathbf{n})$ and $K(\mathbb{C}, \mathbf{n})$, equivalently describe an anisotropic stiffness \mathbb{C} . The direction-dependent Young's modulus $E(\mathbb{C}, \mathbf{n})$ defined by

$$E(\mathbb{C}, \mathbf{n}) = \frac{\sigma(\mathbf{n})}{\varepsilon(\mathbf{n})} = \left[\frac{\varepsilon(\mathbf{n})}{\sigma(\mathbf{n})} \right]^{-1} = \left[\frac{\mathbf{n}^{\otimes 2} \cdot \varepsilon(\mathbf{n})}{\sigma(\mathbf{n})} \right]^{-1}$$

$$= \left[\frac{\mathbf{n}^{\otimes 2} \cdot \mathbb{C}^{-1} [\sigma(\mathbf{n})]}{\sigma(\mathbf{n})} \right]^{-1} = [\mathbb{C}^{-1} \cdot \mathbf{n}^{\otimes 4}]^{-1} \quad (61)$$

represents the ratio of the tensile stress $\sigma(\mathbf{n})$ and the tensile strain $\varepsilon(\mathbf{n})$ during a tensile test in direction \mathbf{n} . The tensile stress caused by a virtual unidirectional tensile test into direction \mathbf{n} , is related to the stress tensor $\sigma(\mathbf{n})$ by $\sigma(\mathbf{n}) = \sigma \mathbf{n}^{\otimes 2} = \sigma \mathbf{n} \otimes \mathbf{n}$. The tensile strain $\varepsilon(\mathbf{n})$ is obtained by a projection of the infinitesimal strain tensor ε onto the direction \mathbf{n} , i.e., $\varepsilon = \varepsilon \cdot \mathbf{n}^{\otimes 2}$. Following He and Curnier (1995) and Böhlke and Brüggemann (2001), the generalized bulk modulus $K(\mathbb{C}, \mathbf{n})$ is defined by

$$3K(\mathbb{C}, \mathbf{n}) = \left[\frac{\mathbf{I} \cdot \varepsilon(\mathbf{n})}{\sigma(\mathbf{n})} \right]^{-1} = \left[\frac{\mathbf{I} \cdot \mathbb{C}^{-1} [\sigma(\mathbf{n})]}{\sigma(\mathbf{n})} \right]^{-1} = [\mathbf{I} \cdot \mathbb{C}^{-1} [\mathbf{n}^{\otimes 2}]]^{-1} \quad (62)$$

and measures the relative change of volume $\mathbf{I} \cdot \varepsilon = [dV - dV_0] / dV_0$ caused by uniaxial tension in direction \mathbf{n} , i.e., $\sigma = \sigma \mathbf{n}^{\otimes 2}$. For a given stiffness \mathbb{C} , both $E(\mathbb{C}, \mathbf{n})$ and $K(\mathbb{C}, \mathbf{n})$ are functions on the unit sphere. The influence of $\mathbb{N}^{\text{planar}}$ on the mechanical properties in the \mathbf{v}_1 - \mathbf{v}_2 -plane is investigated by

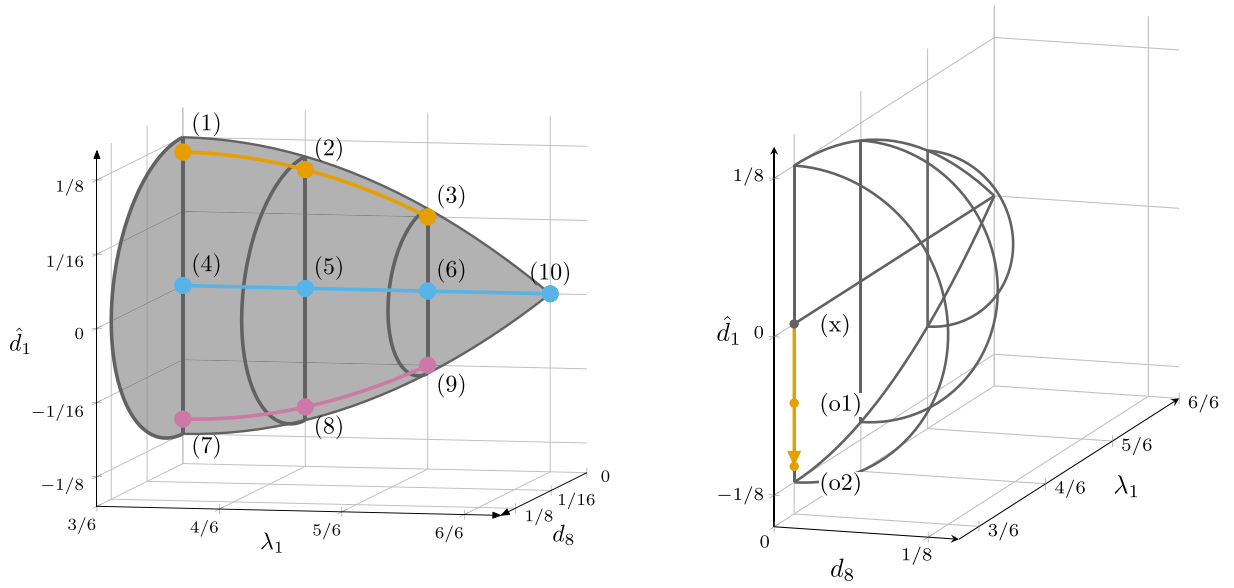
$$E^{\text{planar}}(\mathbb{C}, \varphi) = E(\mathbb{C}, \mathbf{n}(\varphi, \theta = \pi/2)) \quad (63)$$

$$K^{\text{planar}}(\mathbb{C}, \varphi) = K(\mathbb{C}, \mathbf{n}(\varphi, \theta = \pi/2)) \quad (64)$$

with the unit vector $\mathbf{n}(\varphi, \theta)$ specified in Eq. (8). The two quantities $E^{\text{planar}}(\mathbb{C}, \varphi)$ and $K^{\text{planar}}(\mathbb{C}, \varphi)$ uniquely define the mechanical response of the effective stiffness in the plane spanned by \mathbf{v}_1 and \mathbf{v}_2 . Alternative representations of three-dimensional fourth-order tensors are, e.g., given in Vannucci (2018, p. 62).

2.6. Effective stiffnesses: Polar plots and the dependence on planar fourth-order fiber orientations

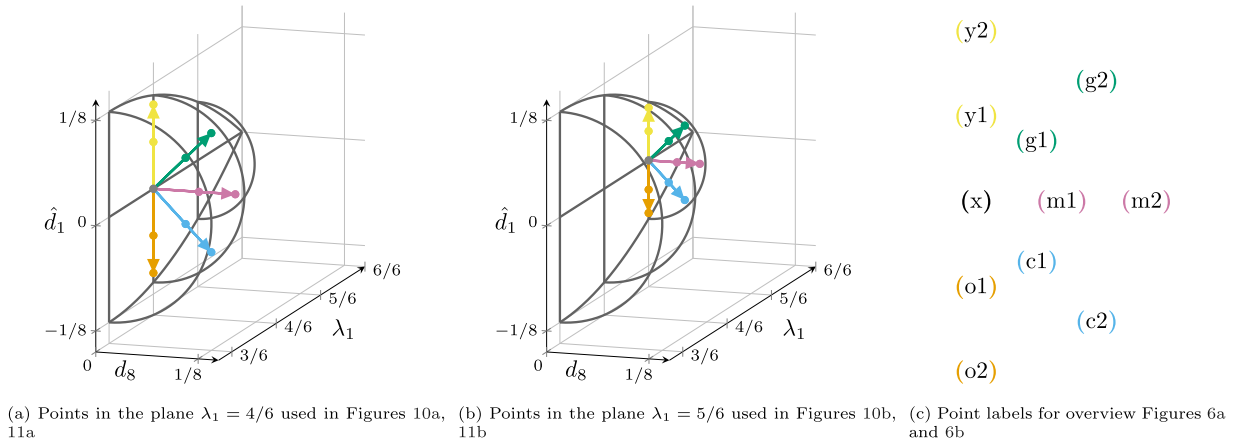
In this section, the building blocks developed in the previous sections are combined to study the dependence of linear elastic effective stiffnesses obtained by mean field homogenization on fourth-order fiber orientation tensors. As the dimensionality of the study is already high due to the flexible orientation, the material parameters of the constituents are fixed and specified in Table 1.



(a) Ten points in the plane of planar orthotropic fiber orientation tensors of fourth-order used in Figures 8a and 8b

(b) Points in the plane $\lambda_1 = 3/6$ used in Figures 9a, 9b

Fig. 5. Definition of representative points in the parameter space $\hat{\mathcal{N}}^{\text{planar}}$ of planar fourth-order fiber orientation tensors.



(a) Points in the plane $\lambda_1 = 4/6$ used in Figures 10a, 11a

(b) Points in the plane $\lambda_1 = 5/6$ used in Figures 10b, 11b

(c) Point labels for overview Figures 6a and 6b

Fig. 6. Definition of representative points in the parameter space $\hat{\mathcal{N}}^{\text{planar}}$ of planar fourth-order fiber orientation tensors. Parameters of each point are listed in Table G.2.

- $\bar{\mathbb{C}}^{\text{HSW2}}(k_1 = 0, k_2 = 0, \mathbb{N}, \dots)$
- $\bar{\mathbb{C}}^{\text{HSW2}}(k_1 = 1, k_2 = 1, \mathbb{N}, \dots)$
- $\bar{\mathbb{C}}^{\text{MTOAB}}(\mathbb{N}, \dots)$
- $\bar{\mathbb{C}}^{\text{MTlinearStiffness}}(\mathbb{N}, \dots)$
- $\bar{\mathbb{C}}^{\text{MTlinearCompliance}}(\mathbb{N}, \dots)$

Fig. 7. Shared legend for Figs. 8–11.

2.6.1. Visualization setup

The space of admissible and distinct planar fourth-order fiber orientations $\mathcal{N}^{\text{planar}}$ is discretized by a small number of representative fiber orientations. Slices through the three-dimensional body $\mathcal{N}^{\text{planar}}$ are defined in Figs. 5(a) to 6(b). On each slice, a number of points, each representing a specific fourth-order fiber orientation tensor $\mathbb{N}^{\text{planar}}$, are selected. For each point, effective stiffnesses are calculated using the orientation averaging homogenization schemes listed in Fig. 7 and described in Section 2.4. The planar properties of each effective stiffness can be visualized by the planar projection of the direction

dependent Young's modulus and generalized bulk modulus, introduced in Section 2.5. In consequence, for each point, two sets of polar plots representing Young's modulus on the one hand and generalized bulk modulus on the other hand, are obtained for a selection of homogenization schemes. Each set of polar plots is combined into one sub-Figure which is arranged according to the position of the point inside the slice of $\mathcal{N}^{\text{planar}}$. This way, a graphical representation of the influence of the fiber orientation on effective stiffnesses is generated. The first slice, visualized in Fig. 5(a), contains ten points, each representing one planar orthotropic (Bauer and Böhlke, 2021, equation (84)) fiber orientation tensor $\mathbb{N}^{\text{planar}}(\lambda_1, \hat{d}_1, d_8)$ with vanishing parameter d_8 defined in Eq. (14). For each point, a polar plot of $E^{\text{planar}}(\bar{\mathbb{C}}(\mathbb{N}), \varphi)$ is given in Fig. 8(a) and a polar plot of $K^{\text{planar}}(\bar{\mathbb{C}}(\mathbb{N}), \varphi)$ is given in Fig. 8(b). The arrangements of the polar plots in Figs. 8(a) and 8(b) mimic the position of the points in the overview Fig. 5(a) and the correspondence is stressed by the color of the thick dashed circles around the polar plots. The line colors of the polar plots indicate the mean field approximation which are specified in the shared legend in Fig. 7. Parameters of each point are given in Table G.2 in Appendix G.

Similar visualizations based on slices in Figs. 5(b) to 6(b) are given in Figs. 9 to 11. Each of the slices in Figs. 5(b) to 6(b) represents

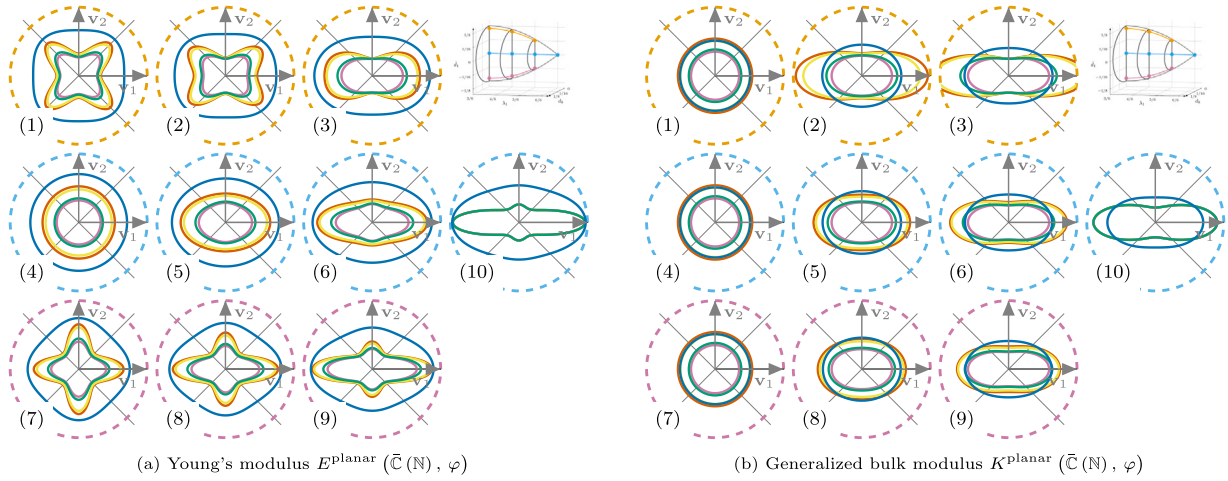


Fig. 8. Polar plots for selected \mathbb{N} specified in Fig. 5(a) and Table G.2 and mean field approximations specified in the legend in Fig. 7.

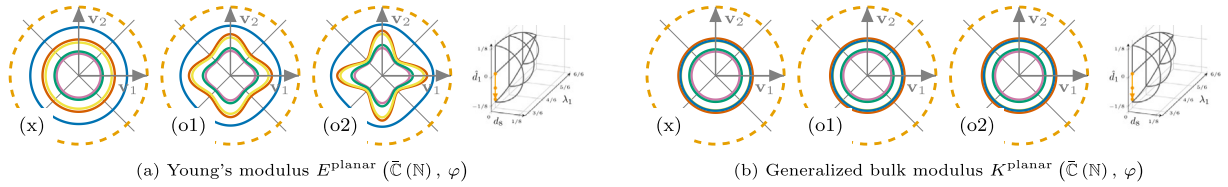


Fig. 9. Polar plots for selected \mathbb{N} with $\lambda_1 = 3/6$ specified in Fig. 5(b) and Table G.2 and mean field approximations specified in the legend in Fig. 7. The order along the path in Fig. 5(b) is given from left to right.

the variety of planar fourth-order fiber orientation tensors for a fixed second-order fiber orientation tensor, as the parameter λ_1 is constant.

The limits of all plots of E^{planar} are homogeneous and given by 0 GPa and 22 GPa. The limits of all plots of K^{planar} are also homogeneous and given by 0 GPa and 24 GPa.

2.6.2. Observations on bounds

In the unidirectional case, visualized in polar plot (10) in Fig. 8(a), all approximations except $\bar{\mathbb{C}}^{\text{HSW}2}(1, 1)$ coincide (Weng, 1990). Young's modulus $E^{\text{planar}}(\bar{\mathbb{C}}, \varphi)$ obtained for the approximations $\bar{\mathbb{C}}^{\text{MTOAB}}$ and $\bar{\mathbb{C}}^{\text{MTLinearStiffness}}$ are between the values obtained for $\bar{\mathbb{C}}^{\text{HSW}2}(0, 0)$ and $\bar{\mathbb{C}}^{\text{HSW}2}(1, 1)$. This does not hold for the approximation $\bar{\mathbb{C}}^{\text{MTLinearCompliance}}$. The limiting two-step Hashin–Shtrikman homogenizations are bounds on the energy of the effective material. Both Young's modulus and the generalized bulk modulus are material characteristics related to uniaxial tensile tests. Motivated by Fig. 8(b)(10), the complementary energy density (Bertram and Glüge, 2013) induced by a virtual direction-dependent unidirectional tensile test starting from a stress-free initial configuration

$$w^*(\bar{\mathbb{C}}, \sigma, \mathbf{n}) = \frac{1}{2} \sigma(\sigma, \mathbf{n}) \cdot \bar{\mathbb{C}}^{-1} [\sigma(\sigma, \mathbf{n})] = \frac{1}{2} \sigma^2 \bar{\mathbb{C}}^{-1} \cdot \mathbf{n}^{\otimes 4} \quad (65)$$

is plotted in Fig. H.12 in Appendix H for a unit stress $\sigma = 1$ and for all views defined in Figs. 5(a) to 6(b). The energies of the approximations $\bar{\mathbb{C}}^{\text{MTOAB}}$ and $\bar{\mathbb{C}}^{\text{MTLinearStiffness}}$ are within the bounds for all inspected orientation tensors whereas the approximation $\bar{\mathbb{C}}^{\text{MTLinearCompliance}}$ violates the bounds and therefore is non-physical.

2.6.3. Observations on the shape of the Young's modulus

The maximum number of extrema of the Young's modulus E^{planar} within the $v_1 - v_2$ -plane is four, as this quantity is obtained by contraction of the effective compliance with a fourth-order moment. The maximum values of the Young's modulus for all mean field approximations point into the directions of maximum fiber content, which are visualized in Bauer and Böhlke (2022). For example, polar plots with $\hat{\beta} = -\pi/2$, i.e., $d_8 = 0$ and $d_1 \leq 0$, have their maxima aligned with the axes v_1 or v_2 , see Figs. 10(a) and 10(b).

2.6.4. Observations on the shape of the generalized bulk modulus

In contrast to the Young's modulus, the number of maxima of the generalized bulk modulus K^{planar} and the resulting shapes are strongly limited, as the highest moment of \mathbf{n} which enters K^{planar} is of second order, see Böhlke and Brüggemann (2001). The changes in K^{planar} for fixed second-order fiber orientation tensor contribution, i.e., fixed values of λ_1 , but different fourth-order fiber orientation tensor contribution, i.e., values of \hat{d}_1 and d_8 defining $\text{dev}(\mathbb{N}^{\text{planar}})$, are marginal for the selected approximations $\bar{\mathbb{C}}^{\text{HSW}2}(k_1, k_2)$ and $\bar{\mathbb{C}}^{\text{MTLinearCompliance}}$. These three approximations take the orientation average on compliance-like quantities. In contrast, the influence of both \hat{d}_1 and d_8 on the remaining approximations $\bar{\mathbb{C}}^{\text{MTOAB}}$ and $\bar{\mathbb{C}}^{\text{MTLinearStiffness}}$ is clearly visible. The latter two approximations take the orientation average on stiffness-like quantities. For these approximations, increase of d_8 induces a clockwise rotation of the K^{planar} -body whereas increase of \hat{d}_1 leads to a stretch of this body. In Fig. 9(b), no stretch is induced by increase of \hat{d}_1 . It is noted, that E^{planar} and K^{planar} are obtained by contraction of the effective compliance. The strong influence of the fourth-order fiber orientation contribution $\text{dev}(\mathbb{N}^{\text{planar}})$ on the shape of the bulk modulus for the approximations $\bar{\mathbb{C}}^{\text{MTOAB}}$ and $\bar{\mathbb{C}}^{\text{MTLinearStiffness}}$ is subject of further research.

2.6.5. Implications of closure approximations based on second-order orientation tensors

Closure approximations (Advani and Tucker III, 1990; Han and Im, 1999; Cintra and Tucker III, 1995; Chung and Kwon, 2002; Montgomery-Smith et al., 2011) identify a fourth-order fiber orientation tensor which corresponds to a given second-order fiber orientation tensor. As any second-order orientation tensor is orthotropic or has even stronger material symmetry, closure approximations based on a second-order orientation tensor lead to orthotropic fourth-order fiber orientation tensors. In consequence, any virtual process chain which involves a closure approximation is limited to orthotropic effective stiffnesses. The planar orthotropic subspace is discretized in Fig. 5(a) and discussed in Bauer and Böhlke (2021). Among the discrete stiffnesses represented in Figs. 10 and 11 only the left column, i.e., those stiffnesses labeled (y2), (y1), (x), (o1), (o2), are orthotropic.

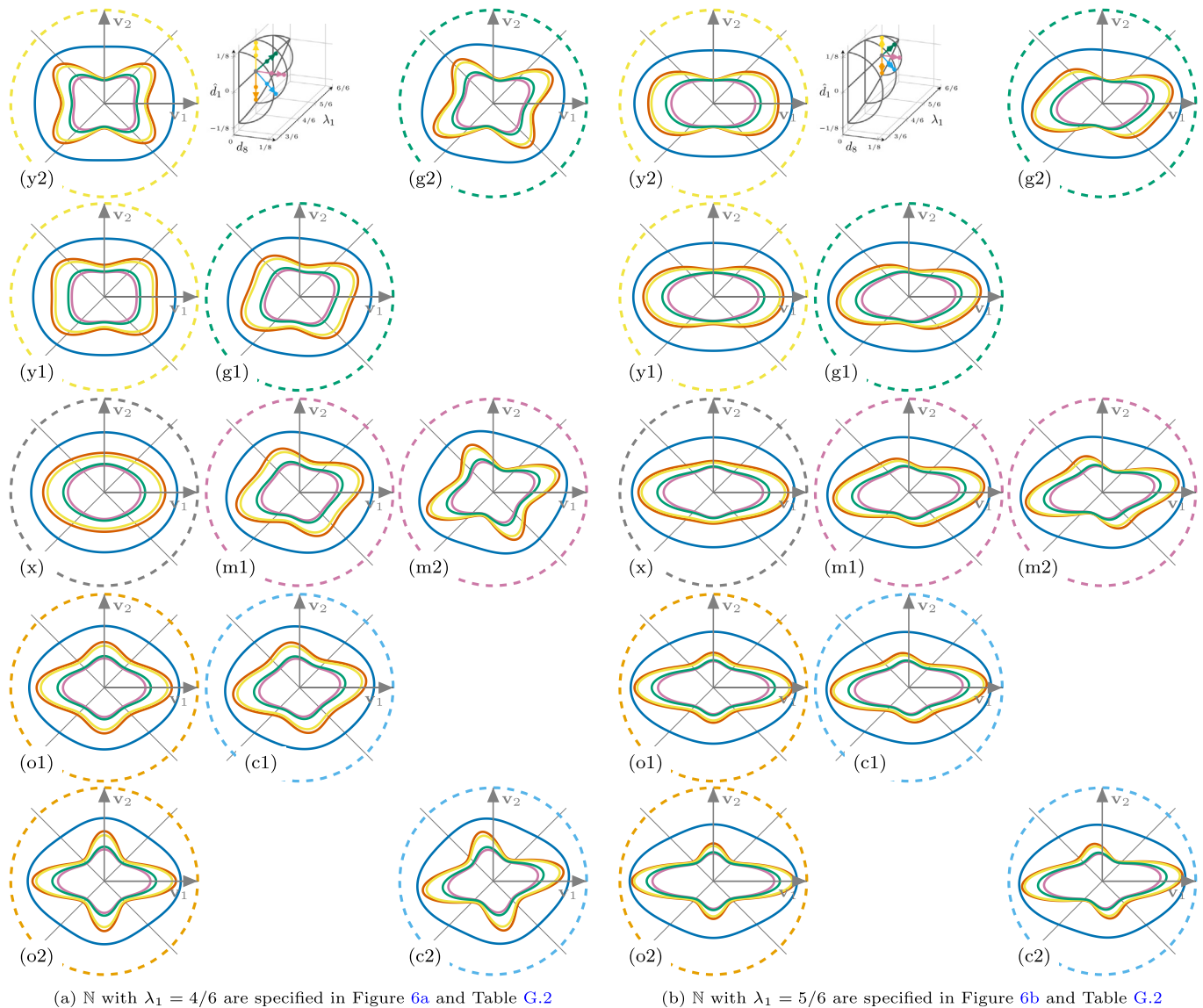


Fig. 10. Young's modulus $E^{\text{planar}}(\bar{\mathbb{C}}(\mathbb{N}), \varphi)$ for mean field approximations specified in Fig. 7. The arrangement of the polar plots follows the arrangement of points in the parameter space of $\mathbb{N}^{\text{planar}}$ in Figs. 6(a) and 6(b).

3. Summary and conclusions

Computer tomography scans combined with knowledge on the variety of fiber orientation tensors and experience in process simulation, reveal that fiber architectures of sheet molding compound specimen are approximately planar. The planarity assumption significantly reduces the dimensionality of the space of fiber orientation tensors from eleven to three in the orientation coordinate system (Bauer and Böhlke, 2021). An invariant and redundancy-free parameter set of structurally differing fiber orientation tensors following Bauer and Böhlke (2022) states the main building block for investigations on the influence of fiber orientation tensors on effective mechanical properties.

The orientation average of transversely isotropic elasticity tensors following Advani and Tucker III (1987) formulated directly in fiber orientation tensors, is explicitly recast as linear invariant composition in the fiber orientation tensors of second and fourth order Kanatani (1984) third kind. To the best of the authors knowledge, this essential assumption of the popular orientation average is not mentioned explicitly in literature. It should be noted, that, e.g., in the field of biomechanics, material models being non-linear in fabric tensors (Cowin, 1985; Turner and Cowin, 1987; Biegler and Mehrabadi, 1995; Cowin and Cardoso,

2011), are established. Such models are based on isotropic tensor functions, i.e., representation theory. A numerical orientation averaging scheme restricted to the special class of planar fiber orientations based on a maximum entropy reconstruction of fiber orientation distribution functions following Bauer and Böhlke (2022) is proposed. The new scheme shows fast converges against the exact formulation of Advani and Tucker III (1987) for non-localized fiber orientation tensors which are dominant in sufficiently large fiber arrangements.

Four mean field homogenization approximations are reviewed and investigated. The first two approximations are orientation averaging Mori-Tanaka following Benveniste (1987) and a two step Hashin-Shtrikman homogenization scheme (Kehrer et al., 2020) both in formulations based on the Advani-Tucker orientation average (Advani and Tucker III, 1987). The remaining two approximations are direct Advani-Tucker orientation averages of either a unidirectional stiffness or compliance obtained by the Mori-Tanaka (Mori and Tanaka, 1973) approximation. Effective stiffnesses obtained by the approximations, are visualized by two-dimensional polar plots of Young's and generalized bulk modulus (Böhlke and Brüggemann, 2001). Plots are generated for specific points in the three-dimensional body of structurally differing planar fiber orientation tensors. The developed

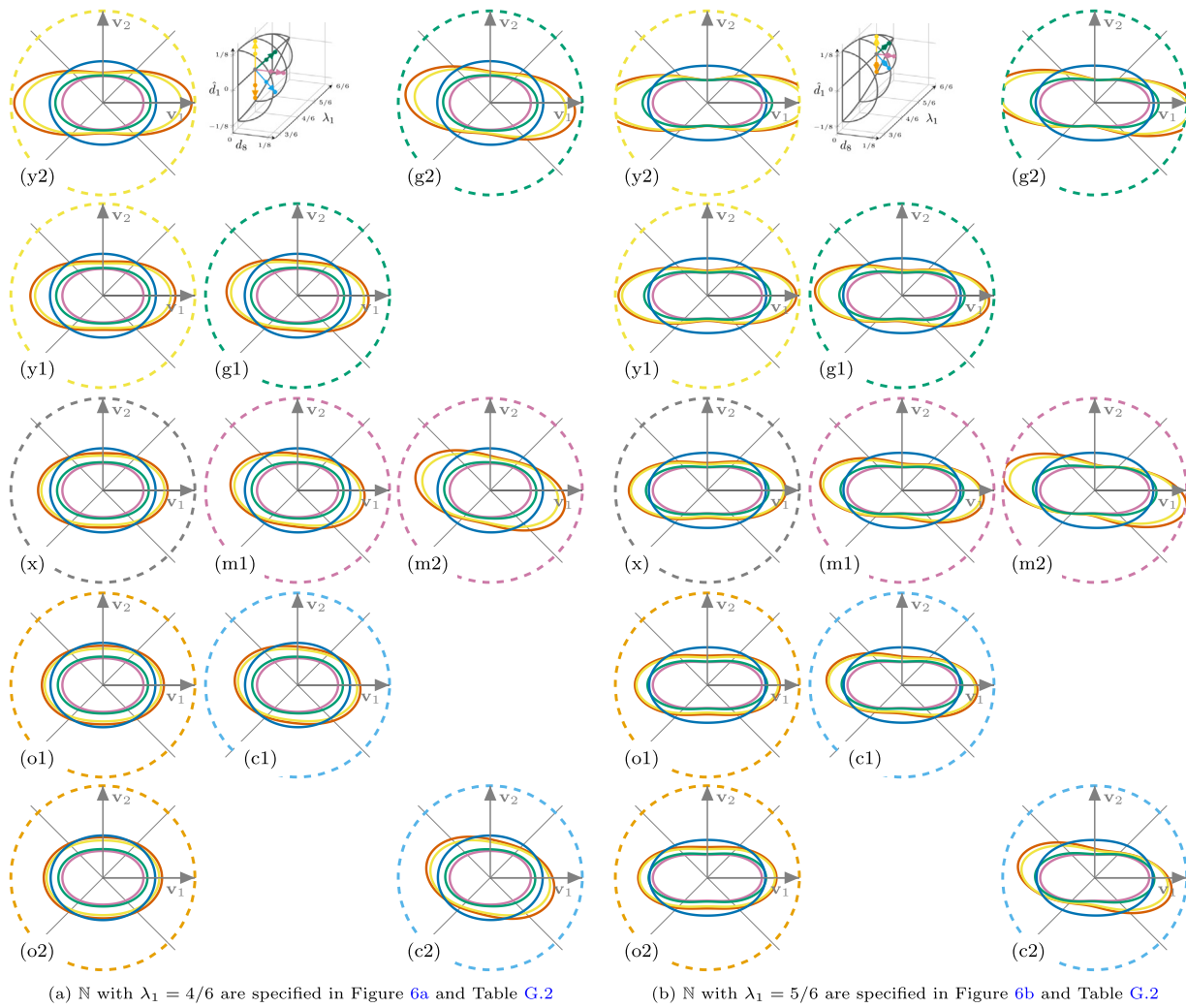


Fig. 11. Generalized bulk modulus $K^{\text{planar}}(\bar{\mathbb{C}}(\mathbb{N}), \varphi)$ for mean field approximations specified in Fig. 7. The arrangement of the polar plots follows the arrangement of points in the parameter space of $\mathbb{N}^{\text{planar}}$ in Figs. 6(a) and 6(b).

views establish a new methodology for studies and visualizations of the dependence of material models on planar fourth-order fiber orientation tensors. Inspection of polar plots of the generalized bulk modulus reveals clear structural differences between effective stiffnesses obtained by mean field schemes taking the orientation average in the stiffness or compliance domain. Those stiffnesses averaged in the compliance domain, hardly show a dependence of the generalized bulk modulus on $\text{dev}(\mathbb{N}^{\text{planar}})$ whereas this dependence is pronounced for stiffnesses averaged in the stiffness domain. The reason for this observation and the physical interpretation of the pronounced dependence is subject of further research. Lack of fourth-order contribution to the generalized bulk modulus (Böhlke and Brüggemann, 2001) restricts the possible shapes of its contour plots. Bauer and Böhlke (2022, Figure 7) visualize reconstructions of fiber orientation distribution functions based on leading fiber orientation tensors up to fourth order. The resulting plots visualize the direct connection between the causing orientation measure and the effected mechanical behavior, e.g., visualized by the effective Young’s modulus in Fig. 10.

The main conclusions of this work are:

- Fiber orientations of sheet molding compound are approximately planar, leading to a reduction of the independent components of fourth-order fiber orientation tensors from eleven to three in the orientation coordinate system.
- An invariant and redundancy-free set of structurally differing fiber orientation tensors of fourth order can be used to investigate the dependence of effective material properties on fiber orientation tensors.
- The orientation average of an elasticity tensor based on a fiber orientation tensor following Advani and Tucker III (1987) is linear in both the elasticity tensor and the fourth-order fiber orientation tensor.
- A new numerical formulation of the Advani–Tucker orientation average in fiber orientation tensors (Advani and Tucker III, 1987) for the special class of planar fiber orientations is proposed based on a maximum entropy reconstruction of fiber orientation distribution functions following Bauer and Böhlke (2022).
- The orientation dependence of the generalized bulk modulus differs significantly for homogenizations which take the orientation average in the stiffness domain and those which take the average in the compliance domain. In contrast, the direction of maxima of the orientation-dependent Young’s modulus is homogeneous for both groups of homogenizations and the difference on the size of the Young’s modulus is barely influenced by the fiber orientation tensor.
- The orientation dependence of the effective anisotropic material response, e.g., described by orientation-dependent Young’s and generalized bulk modulus, is restricted. Restrictions are caused by the limited averaged information given by fourth-order fiber

orientation tensors and due to the constraints of linear elasticity. Possible directional dependencies of the elastic response for Advani–Tucker averaged two-phase materials of isotropic constituents and planar orientation measures are comprehensively presented. This presentation is complete and its methodology states the main contribution of this work. The methodology can be used to express the orientation dependence of any quantity which is a function of planar fiber orientation tensors up to fourth order.

- Orthotropy of closure approximations, which are based on second-order fiber orientation tensors, is shown to be a major restriction on the effective anisotropic material response.

The methodology developed for the low-dimensional subspace of planar fourth-order fiber orientation tensors may be applied to subspaces of fiber orientation tensors with less symmetry.

Abbreviations

FODF	Fiber orientation distribution function
SMC	Sheet molding compound
CT	Computer tomography
RVE	Representative volume element

CRedit authorship contribution statement

Julian Karl Bauer: Conceptualization, Methodology, Software, Validation, Formal analysis, Investigation, Resources, Writing – original draft, Writing – review and editing, Visualization. **Thomas Böhlke:** Methodology, Formal analysis, Resources, Writing – review and editing, Supervision, Project administration, Funding acquisition.

Declaration of competing interest

The authors declare that they have no known competing financial interests or personal relationships that could have appeared to influence the work reported in this paper.

Data availability

The raw/processed data required to reproduce these findings cannot be shared at this time as the data also forms part of an ongoing study.

Acknowledgments

The authors acknowledge inspiring review comment of an anonymous reviewer. CT scans obtained from Ludwig Schöttl are gratefully acknowledged. JKB acknowledges Nils Meyer for valuable intensive technical discussions. JKB acknowledges Jonas Hund for valuable support and discussions on visualizations.

All authors have read and agreed to the published version of the manuscript.

Funding

The research documented in this manuscript has been funded by the German Research Foundation (DFG) within the International Research Training Group “Integrated engineering of continuous–discontinuous long fiber-reinforced polymer structures” (GRK 2078/2). The support by the German Research Foundation (DFG) is gratefully acknowledged.

Code

Selected parts of the source code, this work is based on, are available at [Bauer \(2022\)](#).

Appendix A. Kelvin–Mandel notation and completely symmetric tensors of fourth order

This appendix directly follows (Bauer and Böhlke, 2021, 2022) for the current work to be self-contained. Kelvin–Mandel notation, explicitly introduced in Mandel (1965), originating from Thomson (1856), discussed in Mehrabadi and Cowin (1990), Cowin and Mehrabadi (1992) and Böhlke (2001) and also known as normalized Voigt notation, enables compact two-dimensional representations of fourth-order tensors with at least minor symmetry. A fourth-order tensor $\mathbb{A} = A_{ijkl} \mathbf{e}_i \otimes \mathbf{e}_j \otimes \mathbf{e}_k \otimes \mathbf{e}_l$ is minor symmetric if it has both minor symmetries, i.e., $A_{ijkl} = A_{jikl} = A_{ijlk}$ holds. Introducing base tensors in an arbitrary Cartesian basis $\{\mathbf{e}_i\}$ by

$$\begin{aligned} \mathbf{B}_1 &= \mathbf{e}_1 \otimes \mathbf{e}_1, & \mathbf{B}_4 &= \frac{\sqrt{2}}{2} [\mathbf{e}_2 \otimes \mathbf{e}_3 + \mathbf{e}_3 \otimes \mathbf{e}_2], \\ \mathbf{B}_2 &= \mathbf{e}_2 \otimes \mathbf{e}_2, & \mathbf{B}_5 &= \frac{\sqrt{2}}{2} [\mathbf{e}_1 \otimes \mathbf{e}_3 + \mathbf{e}_3 \otimes \mathbf{e}_1], \\ \mathbf{B}_3 &= \mathbf{e}_3 \otimes \mathbf{e}_3, & \mathbf{B}_6 &= \frac{\sqrt{2}}{2} [\mathbf{e}_2 \otimes \mathbf{e}_1 + \mathbf{e}_1 \otimes \mathbf{e}_2], \end{aligned} \quad (\text{A.1})$$

any minor symmetric tensor \mathbb{A} is represented by a six by six matrix of coefficients $A_{\xi\zeta}$

$$\mathbb{A} = A_{ijkl} \mathbf{e}_i \otimes \mathbf{e}_j \otimes \mathbf{e}_k \otimes \mathbf{e}_l = A_{\xi\zeta} \mathbf{B}_\xi \otimes \mathbf{B}_\zeta \quad (\text{A.2})$$

with ξ and ζ summing from 1 to 6. Complete (index) symmetry of a tensor \mathbb{N} implies the structure

$$\mathbb{N} = \left[\begin{array}{ccc|ccc} N_{11}^{(4)} & N_{12}^{(4)} & N_{13}^{(4)} & \sqrt{2}N_{14}^{(4)} & \sqrt{2}N_{15}^{(4)} & \sqrt{2}N_{16}^{(4)} \\ & N_{22}^{(4)} & N_{23}^{(4)} & \sqrt{2}N_{24}^{(4)} & \sqrt{2}N_{25}^{(4)} & \sqrt{2}N_{26}^{(4)} \\ & & N_{33}^{(4)} & \sqrt{2}N_{34}^{(4)} & \sqrt{2}N_{35}^{(4)} & \sqrt{2}N_{36}^{(4)} \\ \hline & & & 2N_{23}^{(4)} & 2N_{36}^{(4)} & 2N_{25}^{(4)} \\ \text{major symmetric} & & & & 2N_{13}^{(4)} & 2N_{14}^{(4)} \\ & & & & & 2N_{12}^{(4)} \end{array} \right] \mathbf{B}_\xi \otimes \mathbf{B}_\zeta. \quad (\text{A.3})$$

As complete symmetry implies major symmetry, the coefficient matrix in Eq. (A.3) is symmetric. In Eq. (A.3) indices of redundant tensor coefficients are colored. The redundancy implies that six coefficients in the upper left quadrant and nine coefficients in the upper right quadrant of the coefficients in Kelvin–Mandel representation define a completely symmetric tensor. This motivates a short hand notation “completely symmetric”, see, e.g. Eq. (11).

Appendix B. Harmonic decomposition of transversely isotropic elasticity tensors

Following Spencer (1982), Lubarda and Chen (2008) and Walpole (1969), any transversely isotropic elasticity tensor can be parameterized by five scalars and a direction \mathbf{q} . For any choice of a non-unique orthonormal coordinate system \mathbf{m}_i with $\mathbf{m}_1 = \mathbf{q}$, there exists a mapping

$$\hat{\mathbf{Q}}(\mathbf{q}) = \mathbf{m}_i \otimes \mathbf{e}_i \quad (\text{B.1})$$

and enables the following representation of a transversely isotropic stiffness

$$\begin{aligned} &\mathbb{C}^{\text{transv}}(h_1, h_2, h_3, h_4, h_5, \mathbf{q}) \\ &= \hat{\mathbf{Q}}(\mathbf{q}) \star \left(\left[\begin{array}{ccccc} C_{11} & C_{12} & C_{12} & 0 & 0 & 0 \\ & C_{22} & C_{23} & 0 & 0 & 0 \\ & & C_{22} & 0 & 0 & 0 \\ & & & C_{22} - C_{23} & 0 & 0 \\ \text{sym} & & & & 2C_{55} & 0 \\ & & & & & 2C_{55} \end{array} \right] \mathbf{B}_\xi \otimes \mathbf{B}_\zeta \right) \end{aligned} \quad (\text{B.2})$$

$$= h_1 \mathbb{P}_1 + h_2 \mathbb{P}_2 + \hat{\mathbf{Q}}(\mathbf{q}) \star [h_3 \mathbb{J}_3 [\mathbf{F}^{\text{transvx}}] + h_4 \mathbb{J}_4 [\mathbf{F}^{\text{transvx}}] + h_5 \mathbb{F}^{\text{transvx}}] \quad (\text{B.3})$$

with transversely isotropic structure tensors (Olive et al., 2018; Müller and Böhlke, 2016; Bauer and Böhlke, 2021)

$$\mathbf{F}^{\text{transvx}} = \text{dev}(\mathbb{N}^{\text{UD}}) = \frac{2}{3} \begin{bmatrix} 1 & 0 & 0 \\ & -1/2 & 0 \\ \text{sym} & & -1/2 \end{bmatrix} \mathbf{e}_i \otimes \mathbf{e}_j \quad (\text{B.4})$$

$$\mathbb{F}^{\text{transvx}} = \text{dev}(\mathbb{N}^{\text{UD}}) = \frac{1}{35} \begin{bmatrix} 8 & -4 & -4 & 0 & 0 & 0 \\ & 3 & 1 & 0 & 0 & 0 \\ & & 3 & 0 & 0 & 0 \\ \hline \text{completely} & & & \text{symmetric} & & \end{bmatrix} \mathbf{B}_\xi \otimes \mathbf{B}_\zeta \quad (\text{B.5})$$

and isotropic sixth order tensors

$$\mathbb{J}_3 = [\delta_{ij} \delta_{km} \delta_{ln} + \delta_{kl} \delta_{im} \delta_{jn}] \mathbf{e}_i \otimes \mathbf{e}_j \otimes \mathbf{e}_k \otimes \mathbf{e}_l \otimes \mathbf{e}_m \otimes \mathbf{e}_n \quad (\text{B.6})$$

$$\mathbb{J}_4 = \frac{1}{8} [\delta_{in} \delta_{jk} \delta_{lm} + \delta_{in} \delta_{jl} \delta_{km} + \delta_{im} \delta_{jk} \delta_{ln} + \delta_{im} \delta_{jl} \delta_{kn} + \delta_{ik} \delta_{jm} \delta_{ln} + \delta_{ik} \delta_{jn} \delta_{lm} + \delta_{il} \delta_{jm} \delta_{kn} + \delta_{il} \delta_{jn} \delta_{km}] \mathbf{e}_i \otimes \mathbf{e}_j \otimes \mathbf{e}_k \otimes \mathbf{e}_l \otimes \mathbf{e}_m \otimes \mathbf{e}_n. \quad (\text{B.7})$$

The scaling factors $2/3$ and $1/35$ of the structure tensors in Eqs. (B.4) and (B.5) do not lead to a norm of value one. This is in contrast to formulations in, e.g., Fernández and Böhlke (2019, Eq. (75)), but leads to a direct connection to unidirectional fiber orientation tensors $\mathbb{N}^{\text{UD}} = \mathbf{v}_i \otimes \mathbf{v}_i$ and $\mathbb{N}^{\text{UD}} = \mathbf{B}_i^v \otimes \mathbf{B}_i^v$ and compact expressions for h_i with $i \in \{1, 2, 3, 4, 5\}$ in Eq. (B.3) which are related to the tensor components in Eq. (B.2) by

$$h_1 = 3K = \frac{1}{3} [C_{11} + 4C_{12} + 2C_{22} + 2C_{23}] \quad (\text{B.8})$$

$$h_2 = 2G = \frac{1}{15} [2C_{11} - 4C_{12} + 7C_{22} - 5C_{23} + 12C_{55}] \quad (\text{B.9})$$

$$h_3 = \frac{1}{7} [C_{11} + 5C_{12} + C_{22} - 7C_{23} - 4C_{55}] \quad (\text{B.10})$$

$$h_4 = \frac{1}{14} [2C_{11} - 4C_{12} - 5C_{22} + 7C_{23} + 6C_{55}] \quad (\text{B.11})$$

$$h_5 = \frac{1}{35} [C_{11} - 2C_{12} + C_{22} - 4C_{55}] \quad (\text{B.12})$$

with the bulk modulus K and the shear modulus G . Eqs. (B.1) to (B.3) motivate a short hand notation for a transversely isotropic elasticity tensor using $[\cdot]$ with

$$\mathbb{C}^{\text{transv}}(h_1, h_2, h_3, h_4, h_5, \mathbf{q}) = [h_1, h_2, h_3, h_4, h_5, \mathbf{q}]. \quad (\text{B.13})$$

Following Rychlewski (2000), Eq. (B.3) represents the classical linear invariant decomposition of a transversely isotropic elasticity tensor into irreducible parts. The classical linear invariant decomposition is one out of an infinite number of possible linear invariant decompositions (Forte and Vianello, 1996; Rychlewski, 2000). Any non-classical linear invariant decomposition leads to a representation of $\mathbb{C}^{\text{transv}}$ which differs from Eq. (B.3) by the set of isotropic tensors $\mathbb{J}_3, \mathbb{J}_4$ and the values of the corresponding coefficients h_3 and h_4 .

Appendix C. Reformulation of the Advani–Tucker orientation average

Listing 1 contains symbolic tensor manipulation code to validate the representation of the Advani–Tucker orientation average in the formulation given in Eq. (16) and which is based on the classical linear invariant decomposition (Rychlewski, 2000).

Appendix D. Advani–Tucker orientation average of minor symmetric tensors

A generic transversely isotropic fourth-order tensor, which has both minor symmetries but lacks major symmetry, i.e., $H_{ijkl} = H_{ijlk} = H_{jikl}$ but $H_{ijkl} \neq H_{klij}$ with $\mathbb{H}^{\text{transv}} = H_{ijkl} \mathbf{e}_i \otimes \mathbf{e}_j \otimes \mathbf{e}_k \otimes \mathbf{e}_l$, depends on a direction \mathbf{q} and six scalars, see Schröder and Gross (2004) and Brannon (2018). For any choice of a non-unique orthonormal coordinate system \mathbf{m}_i with $\mathbf{m}_i = \mathbf{q}$, there exists a mapping

$$\hat{\mathbf{Q}}(\mathbf{q}) = \mathbf{m}_i \otimes \mathbf{e}_i, \quad (\text{D.1})$$

which enables the following representation of a transversely isotropic minor symmetric fourth-order tensor lacking the major symmetry

$$\mathbb{H}^{\text{transv}}(H_{11}, H_{22}, H_{12}, H_{21}, H_{23}, H_{55}, \mathbf{q}) = \hat{\mathbf{Q}}(\mathbf{q}) \star \left(\begin{bmatrix} H_{11} & H_{12} & H_{12} & 0 & 0 & 0 \\ H_{21} & H_{22} & H_{23} & 0 & 0 & 0 \\ H_{21} & H_{23} & H_{22} & 0 & 0 & 0 \\ 0 & 0 & 0 & H_{22} - H_{23} & 0 & 0 \\ 0 & 0 & 0 & 0 & 2H_{55} & 0 \\ 0 & 0 & 0 & 0 & 0 & 2H_{55} \end{bmatrix} \mathbf{B}_\xi \otimes \mathbf{B}_\zeta \right). \quad (\text{D.2})$$

In other words, if the transversely isotropic axis is aligned with the \mathbf{e}_1 -axis of the coordinate system underlying the Kelvin–Mandel basis $\mathbf{B}_\xi \otimes \mathbf{B}_\zeta$ in Eq. (D.2), the matrix representation of Kelvin–Mandel components has the simplified structure shown in Eq. (D.2). Compared to the representation of $\mathbb{C}^{\text{transv}}$ in Eq. (B.2), lack of the major symmetry of $\mathbb{H}^{\text{transv}}$ results in one additional independent tensor component in Eq. (D.2). In order to extend the reformulation of the Advani–Tucker orientation average in Eq. (16) to tensors which lack the major symmetry, harmonic decomposition (Forte and Vianello, 1996; Rychlewski, 2000) of such tensors is investigated following Fernández and Böhlke (2019, Section 2.4) and Lobos et al. (2017, Appendix A). Lack of major symmetry of a minor symmetric fourth-order tensor, potentially adds three additional subspaces of orders one, two and three, to the subspaces of its harmonic decomposition. If the decomposed quantity is major symmetric, the contributions of these three additional subspaces are zero (Lobos et al., 2017, Section 2.4). It is easy to show, that no non-vanishing first-order tensor \mathbf{a} fulfills

$$\mathbf{Q} \star \mathbf{a} = \mathbf{a} \quad \forall \quad \mathbf{Q} \in \mathcal{S}^{\text{transv}} \quad (\text{D.3})$$

with the transversely isotropic symmetry group $\mathcal{S}^{\text{transv}}$. Following Brannon (2018), the same holds for harmonic tensors of third order. In consequence, the additional degree of freedom of $\mathbb{H}^{\text{transv}}$ in Eq. (D.2) compared to $\mathbb{C}^{\text{transv}}$ in Eq. (B.2) corresponds to the additional subspace of second order in the harmonic decomposition of minor symmetric fourth-order tensors which lack major symmetry. As the symmetry group of a tensor is the intersection of the symmetry groups of its harmonic parts (Forte and Vianello, 1996), transversely isotropy of $\mathbb{H}^{\text{transv}}$ demands that this subspace is also transversely isotropic, making it one-dimensional and being a multiple of a structure tensor $\mathbf{F}^{\text{transvx}}$ defined in Eq. (B.4). Consequently, $\mathbb{H}^{\text{transv}}$ can be represented by extending Eq. (B.3) to

$$\mathbb{H}^{\text{transv}}(h_1, h_2, h_3, h_4, h_5, h_6, \mathbf{q}) = h_1 \mathbb{P}_1 + h_2 \mathbb{P}_2 + \hat{\mathbf{Q}}(\mathbf{q}) \star [h_3 \mathbb{J}_3 [\mathbf{F}^{\text{transvx}}] + h_4 \mathbb{J}_4 [\mathbf{F}^{\text{transvx}}] + h_5 \mathbb{F}^{\text{transvx}} + h_6 \mathbb{J}_6 [\mathbf{F}^{\text{transvx}}]] \quad (\text{D.4})$$

with $\mathbf{F}^{\text{transvx}}, \mathbb{F}^{\text{transvx}}, \mathbb{J}_3$ and \mathbb{J}_4 defined in Eqs. (B.4) to (B.7) and with the isotropic sixth-order tensor

$$\mathbb{J}_6 = [-\delta_{ij} \delta_{kn} \delta_{lm} + \delta_{in} \delta_{jm} \delta_{kl}] \mathbf{e}_i \otimes \mathbf{e}_j \otimes \mathbf{e}_k \otimes \mathbf{e}_l \otimes \mathbf{e}_m \otimes \mathbf{e}_n \quad (\text{D.5})$$

following Fernández and Böhlke (2019), acting as

$$\mathbb{J}_6[\mathbf{H}] = -\mathbf{I} \otimes \mathbf{H} + \mathbf{H} \otimes \mathbf{I}. \quad (\text{D.6})$$

Listing 1: Validation of the orientation average following Advani and Tucker III (1987) given in Eq. (16)

```

1 import sympy as sp
2 import symbolic as sb
3
4
5 D2 = sb.fabric_tensor.dev2_by_la0_la1()
6 D4 = sb.fabric_tensor.dev4_triclinic_by_d()
7 N4 = sb.special.combine_to_N4(D2=D2, D4=sb.tensorr(D4))
8
9 # eq. (88) Transvsely isotropic stiffness
10 stiffness = sb.material_symmetry.transversely_isotropic_x_minimal_harmonic_normalized(
11     normalization="structure_tensor_multiplicity"
12 )
13
14 print("Orientation tensor fourth-order Kanatani first kind =\n", N4)
15 print("Transversely isotropic stiffness =\n", stiffness)
16
17 averager = sb.orientation_average.AdvaniTucker(N4=N4)
18 average = averager.average(stiffness)
19
20 decomposer_Rych = sb.elasticity.Rychlewski2000()
21 decomposition = decomposer_Rych.decompose_classical_harmonic(
22     stiffness=sb.tensorr(average)
23 )["parts"]
24
25
26 def test_equality(A, B):
27     return sp.simplify(A) == sp.simplify(B)
28
29
30 assert test_equality(decomposition["h1"], sb.abc.h1)
31 assert test_equality(decomposition["h2"], sb.abc.h2)
32 assert test_equality(decomposition["H1"], D2 * sb.abc.h3)
33 assert test_equality(decomposition["H2"], D2 * sb.abc.h4)
34 assert test_equality(sb.mandel(decomposition["H"]), D4 * sb.abc.h5)

```

The connection between h_i for $i \in [1, 2, 3, 4, 5]$ and components H_{ij} in Eq. (D.2) follows the pattern in Eqs. (B.8) to (B.12) combined with

$$h_6 = \frac{1}{2} (H_{12} - H_{21}). \quad (\text{D.7})$$

Based on the representation of $\mathbb{H}^{\text{transv}}$ in Eq. (D.4), the Advani-Tucker (Advani and Tucker III, 1987) orientation average given in Eq. (16) can be extended to minor symmetric fourth-order tensors which lack the major symmetry, leading to

$$\begin{aligned} \langle \mathbb{H}^{\text{transv}}(h_1, h_2, h_3, h_4, h_5, h_6, \mathbf{q}) \rangle_{\text{ATN}}(\mathbb{N}) &= h_1 \mathbb{P}_1 + h_2 \mathbb{P}_2 \\ &+ h_3 \mathbb{J}_3 [\text{dev}(\mathbb{N})] \\ &+ h_4 \mathbb{J}_4 [\text{dev}(\mathbb{N})] \\ &+ h_5 \text{dev}(\mathbb{N}) \\ &+ h_6 \mathbb{J}_6 [\text{dev}(\mathbb{N})] \end{aligned} \quad (\text{D.8})$$

with $\text{dev}(\mathbb{N})$, $\text{dev}(\mathbb{N})$ defined in Eqs. (17) and (18). An alternative representation closely following the original formulation of Advani-Tucker (Advani and Tucker III, 1987) is given by

$$\begin{aligned} (\langle \mathbb{H}^{\text{transv}} \rangle_{\text{ATN}})_{ijkl} &= b_1 N_{ijkl}^{(4)} \\ &+ b_2 N_{ij} \delta_{kl} + b_6 N_{kl} \delta_{ij} \\ &+ b_3 (N_{ij} \delta_{jl} + N_{il} \delta_{jk} + N_{jl} \delta_{ik} + N_{jk} \delta_{il}) \\ &+ b_4 \delta_{ij} \delta_{kl} + b_5 (\delta_{ik} \delta_{jl} + \delta_{il} \delta_{jk}) \end{aligned} \quad (\text{D.9})$$

with component representations in an arbitrary coordinate system

$$\mathbb{N} = N_{ijkl}^{(4)} \mathbf{e}_i \otimes \mathbf{e}_j \otimes \mathbf{e}_k \otimes \mathbf{e}_l \quad (\text{D.10})$$

$$\mathbb{N} = N_{ij} \mathbf{e}_i \otimes \mathbf{e}_j. \quad (\text{D.11})$$

The coefficients b_i for $i \in [1, 2, 3, 4, 5, 6]$ are defined by

$$b_1 = H_{1111} + H_{2222} - H_{1122} - H_{2211} - 4H_{1212} \quad (\text{D.12})$$

$$b_2 = H_{1122} - H_{2233} \quad (\text{D.13})$$

$$b_3 = H_{1212} + \frac{1}{2} (H_{2233} - H_{2222}) \quad (\text{D.14})$$

$$b_4 = H_{2233} \quad (\text{D.15})$$

$$b_5 = H_{2222} - H_{2233} \quad (\text{D.16})$$

$$b_6 = H_{2211} - H_{2233} \quad (\text{D.17})$$

based on tensor components of $\mathbb{H}^{\text{transv}} = H_{ijkl} \mathbf{e}_i \otimes \mathbf{e}_j \otimes \mathbf{e}_k \otimes \mathbf{e}_l$ in a coordinate system with \mathbf{e}_1 aligned along the transversely isotropic axis of $\mathbb{H}^{\text{transv}}$, i.e., the tensor components H_{ijkl} are directly related to the Kelvin-Mandel components H_{ij} in Eq. (D.2). If the quantity to be averaged is major symmetric, the coefficients in Eqs. (D.12) to (D.17) coincide with those for the original formulation (Advani and Tucker III, 1987), e.g., given in Brylka (2017, Eq. (2.89)) or (Kehrer et al., 2020, Eq. (27)).

Appendix E. Connection to notation in Kehrer et al. (2020)

The two-step scheme in Eqs. (32) and (33) simplifies to the one proposed in Kehrer et al. (2020), if $k_1 = 0$ or $k_1 = 1$ and $k_2 = k$. Eqs. (E.1) and (E.2) connect the notation of this work on the left hand side and the notation of Kehrer et al. (2020) on the right hand by

$$\bar{\mathbb{C}}^{\text{HSW2}}(k_1 = 0, k_2 = k, \dots) \triangleq \bar{\mathbb{C}}^{\text{HS-}}(k), \quad (\text{E.1})$$

$$\bar{\mathbb{C}}^{\text{HSW2}}(k_1 = 1, k_2 = k, \dots) \triangleq \bar{\mathbb{C}}^{\text{HS+}}(k). \quad (\text{E.2})$$

Appendix F. Component representations of tensor inversions

Explicit representations of components after matrix inversion in Eq. (42) are given by

$$h_1^{\text{B}} = 3 (105h_2 + 140h_4 + 36h_5) / b_1 \quad (\text{F.1})$$

$$\begin{aligned} h_2^{\text{B}} &= 105 (33075h_1h_2^2 + 22050h_1h_2h_4 + 5670h_1h_2h_5 - 17640h_1h_4^2 \\ &- 3780h_1h_4h_5 - 864h_1h_5^2 - 52920h_2h_3^2 - 141120h_2h_3h_4 \\ &- 94080h_2h_4^2 + 17640h_3^2h_4 + 4536h_3^2h_5 + 47040h_3h_4^2 \\ &+ 12096h_3h_4h_5 + 31360h_4^3 + 8064h_4^2h_5) / (b_1b_2) \quad (\text{F.2}) \\ h_3^{\text{B}} &= 45 (102900h_1h_2h_4 + 98000h_1h_4^2 - 2520h_1h_4h_5 - 3600h_1h_5^2 \\ &- 77175h_2^2h_3 - 102900h_2^2h_4 - 44100h_2h_3^2 - 66150h_2h_3h_4 \end{aligned}$$

Table G.2

Parameter combinations leading to selected fourth-order fiber orientation tensors, which are used to generate polar plots in Figs. 8, 9, 10 and 11. The corresponding parameterization $\mathbb{N}^{\text{planar}}(\lambda_1, \hat{r}, \hat{\beta})$ is defined in Eq. (11). Numerical values of the Lagrange multipliers (L, f_1, f_2, g_1, g_2) specifying $\hat{\psi}^{\text{ME}}(\varphi_i, \mathbb{N}^{\text{planar}})$ following Bauer and Böhlke (2022, equation (71)) are given with absolute values smaller than $10^{-5} = 1\text{E}^{-5}$ set to zero.

Figures	λ_1	$\hat{\beta}$	\hat{r}	L	f_1	f_2	g_1	g_2
8(a)(1), 8(b)(1)	1/2	$\pi/2$	9/80	4.42E ⁰	0	0	-5.30E ⁰	0
8(a)(2), 8(b)(2)	2/3	$\pi/2$	1/10	6.43E ⁰	-7.69E ⁰	0	-6.12E ⁰	0
8(a)(3), 8(b)(3)	5/6	$\pi/2$	1/16	1.66E ¹	-2.46E ¹	0	-9.77E ⁰	0
8(a)(4), 8(b)(4)	1/2	0	0	8.38E ⁻¹	0	0	0	0
8(a)(5), 8(b)(5)	2/3	0	0	9.56E ⁻¹	-6.67E ⁻¹	0	1.20E ⁻¹	0
8(a)(6), 8(b)(6)	5/6	0	0	1.45E ⁰	-1.34E ⁰	0	6.49E ⁻¹	0
8(a)(7), 8(b)(7)	1/2	$-\pi/2$	9/80	4.42E ⁰	0	0	5.30E ⁰	0
8(a)(8), 8(b)(8)	2/3	$-\pi/2$	1/10	5.01E ⁰	-3.63E ⁻¹	0	5.89E ⁰	0
8(a)(9), 8(b)(9)	5/6	$-\pi/2$	1/16	8.26E ⁰	-8.34E ⁻¹	0	9.13E ⁰	0
8(a)(10), 8(b)(10)	1	0	0	1.81E ³	-5.51E ⁰	1.03E ¹	1.81E ³	-5.18E ⁰
9(a)(x), 9(b)(x)	1/2	0	0	8.38E ⁻¹	0	0	0	0
9(a)(o1), 9(b)(o1)	1/2	$-\pi/2$	1/16	1.15E ⁰	0	0	1.16E ⁰	0
9(a)(o2), 9(b)(o2)	1/2	$-\pi/2$	9/80	4.42E ⁰	0	0	5.30E ⁰	0
10(a)(x), 11(a)(x)	2/3	0	0	9.56E ⁻¹	-6.67E ⁻¹	0	1.20E ⁻¹	0
10(a)(o1), 11(a)(o1)	2/3	$-\pi/2$	1/18	1.30E ⁰	-4.54E ⁻¹	0	1.30E ⁰	0
10(a)(o2), 11(a)(o2)	2/3	$-\pi/2$	1/10	5.01E ⁰	-3.63E ⁻¹	0	5.89E ⁰	0
10(a)(c1), 11(a)(c1)	2/3	$-\pi/4$	1/18	1.31E ⁰	-5.86E ⁻¹	3.36E ⁻¹	9.53E ⁻¹	-8.36E ⁻¹
10(a)(c2), 11(a)(c2)	2/3	$-\pi/4$	1/10	5.20E ⁰	-1.39E ⁰	2.51E ⁰	4.22E ⁰	-4.15E ⁰
10(a)(m1), 11(a)(m1)	2/3	0	1/18	1.32E ⁰	-9.01E ⁻¹	4.71E ⁻¹	1.20E ⁻¹	-1.19E ⁰
10(a)(m2), 11(a)(m2)	2/3	0	1/10	5.69E ⁰	-3.93E ⁰	3.60E ⁰	8.21E ⁻²	-5.99E ⁰
10(a)(g1), 11(a)(g1)	2/3	$\pi/4$	1/18	1.33E ⁰	-1.21E ⁰	3.30E ⁻¹	-7.18E ⁻¹	-8.40E ⁻¹
10(a)(g2), 11(a)(g2)	2/3	$\pi/4$	1/10	6.21E ⁰	-6.56E ⁰	2.59E ⁰	-4.26E ⁰	-4.35E ⁰
10(a)(y1), 11(a)(y1)	2/3	$\pi/2$	1/18	1.33E ⁰	-1.33E ⁰	0	-1.07E ⁰	0
10(a)(y2), 11(a)(y2)	2/3	$\pi/2$	1/10	6.43E ⁰	-7.69E ⁰	0	-6.12E ⁰	0
10(b)(x), 11(b)(x)	5/6	0	0	1.45E ⁰	-1.34E ⁰	0	6.49E ⁻¹	0
10(b)(o1), 11(b)(o1)	5/6	$-\pi/2$	5/144	2.00E ⁰	-9.88E ⁻¹	0	1.96E ⁰	0
10(b)(o2), 11(b)(o2)	5/6	$-\pi/2$	1/16	8.26E ⁰	-8.34E ⁻¹	0	9.13E ⁰	0
10(b)(c1), 11(b)(c1)	5/6	$-\pi/4$	5/144	2.04E ⁰	-1.29E ⁰	9.33E ⁻¹	1.59E ⁰	-9.71E ⁻¹
10(b)(c2), 11(b)(c2)	5/6	$-\pi/4$	1/16	9.37E ⁰	-4.00E ⁰	7.92E ⁰	6.69E ⁰	-6.27E ⁰
10(b)(m1), 11(b)(m1)	5/6	0	5/144	2.07E ⁰	-1.93E ⁰	1.25E ⁰	6.77E ⁻¹	-1.36E ⁰
10(b)(m2), 11(b)(m2)	5/6	0	1/16	1.23E ¹	-1.20E ¹	1.17E ¹	5.68E ⁻¹	-9.41E ⁰
10(b)(g1), 11(b)(g1)	5/6	$\pi/4$	5/144	1.95E ⁰	-2.37E ⁰	7.97E ⁻¹	-1.91E ⁻¹	-9.20E ⁻¹
10(b)(g2), 11(b)(g2)	5/6	$\pi/4$	1/16	1.55E ¹	-2.09E ¹	8.87E ⁰	-6.48E ⁰	-7.31E ⁰
10(b)(y1), 11(b)(y1)	5/6	$\pi/2$	5/144	1.86E ⁰	-2.47E ⁰	0	-5.16E ⁻¹	0
10(b)(y2), 11(b)(y2)	5/6	$\pi/2$	1/16	1.66E ¹	-2.46E ¹	0	-9.77E ⁰	0

$$\begin{aligned}
 &+ 13230h_2h_3h_5 - 9800h_2h_4^2 + 17640h_2h_4h_5 - 117600h_3^2h_4 \\
 &+ 22680h_3^2h_5 - 245000h_3h_4^2 + 34020h_3h_4h_5 + 1008h_3h_5^2 \\
 &- 117600h_4^3 + 5040h_4^2h_5 + 1344h_4h_5^2 / (b_1b_2) \quad (\text{F.3})
 \end{aligned}$$

$$\begin{aligned}
 h_4^B = &-225 (15435h_1h_2h_4 + 14700h_1h_4^2 - 378h_1h_4h_5 - 540h_1h_5^2 \\
 &- 6615h_2h_3^2 - 17640h_2h_3h_4 - 11760h_2h_4^2 - 17640h_3^2h_4 + 3402h_3^2h_5 \\
 &- 47040h_3h_4^2 + 9072h_3h_4h_5 - 31360h_4^3 + 6048h_4^2h_5) / (b_1b_2) \quad (\text{F.4})
 \end{aligned}$$

$$\begin{aligned}
 h_5^B = &-1575 (2205h_1h_2h_5 - 5880h_1h_4^2 - 2730h_1h_4h_5 + 216h_1h_5^2 \\
 &- 6615h_2h_3^2 - 17640h_2h_3h_4 - 11760h_2h_4^2 + 13230h_3^2h_4 - 1008h_3^2h_5 \\
 &+ 35280h_3h_4^2 - 2688h_3h_4h_5 + 23520h_4^3 - 1792h_4^2h_5) / (b_1b_2) \quad (\text{F.5})
 \end{aligned}$$

$$b_1 = 315h_1h_2 + 420h_1h_4 + 108h_1h_5 - 630h_3^2 - 1680h_3h_4 - 1120h_4^2 \quad (\text{F.6})$$

$$b_2 = (105h_2 - 140h_4 + 6h_5) (105h_2 + 70h_4 - 24h_5) \quad (\text{F.7})$$

after orientation averaging in Eq. (43) by

$$\begin{aligned}
 E_{11} = &-\frac{1}{35} [35B_{11}d_1 - 35B_{11}\lambda_1 + 4B_{11} - 70B_{12}d_1 - 8B_{12} + 35B_{22}d_1 \\
 &+ 35B_{22}\lambda_1 - 31B_{22} - 140B_{55}d_1 - 16B_{55}] \quad (\text{F.8})
 \end{aligned}$$

$$\begin{aligned}
 E_{12} = &\frac{1}{35} [35B_{11}d_1 + 4B_{11} - 70B_{12}d_1 + 27B_{12} + 35B_{22}d_1 + 4B_{22} \\
 &- 140B_{55}d_1 - 16B_{55}] \quad (\text{F.9})
 \end{aligned}$$

$$E_{13} = B_{12}\lambda_1 - B_{23}\lambda_1 + B_{23} \quad (\text{F.10})$$

$$E_{16} = \sqrt{2}d_8 (B_{11} - 2B_{12} + B_{22} - 4B_{55}) \quad (\text{F.11})$$

$$\begin{aligned}
 E_{22} = &-\frac{1}{35} [35B_{11}d_1 + 35B_{11}\lambda_1 - 31B_{11} - 70B_{12}d_1 - 8B_{12} + 35B_{22}d_1 \\
 &- 35B_{22}\lambda_1 + 4B_{22} - 140B_{55}d_1 - 16B_{55}] \quad (\text{F.12})
 \end{aligned}$$

$$E_{23} = -B_{12}\lambda_1 + B_{12} + B_{23}\lambda_1 \quad (\text{F.13})$$

$$E_{33} = B_{22} \quad (\text{F.14})$$

$$E_{44} = B_{22}\lambda_1 - B_{23}\lambda_1 - 2B_{55}\lambda_1 + 2B_{55} \quad (\text{F.15})$$

$$E_{55} = -B_{22}\lambda_1 + B_{22} + B_{23}\lambda_1 - B_{23} + 2B_{55}\lambda_1 \quad (\text{F.16})$$

$$\begin{aligned}
 E_{66} = &\frac{2}{35} [35B_{11}d_1 + 4B_{11} - 70B_{12}d_1 - 8B_{12} + 35B_{22}d_1 + 4B_{22} \\
 &- 140B_{55}d_1 + 19B_{55}] \quad (\text{F.17})
 \end{aligned}$$

with $d_1 = \hat{d}_1 + R(\hat{\lambda}_1) - \frac{4}{35}$ (see Bauer and Böhlke, 2022) and after matrix inversion in Eq. (44) by

$$G_{11} = \frac{E_{16}^2 E_{33} - E_{22} E_{33} E_{66} + E_{23}^2 E_{66}}{b} \quad (\text{F.18})$$

$$G_{12} = \frac{E_{12} E_{33} E_{66} - E_{13} E_{23} E_{66} + E_{16}^2 E_{33}}{b} \quad (\text{F.19})$$

$$G_{13} = -\frac{E_{12} E_{23} E_{66} + E_{13} E_{16}^2 - E_{13} E_{22} E_{66} + E_{16}^2 E_{23}}{b} \quad (\text{F.20})$$

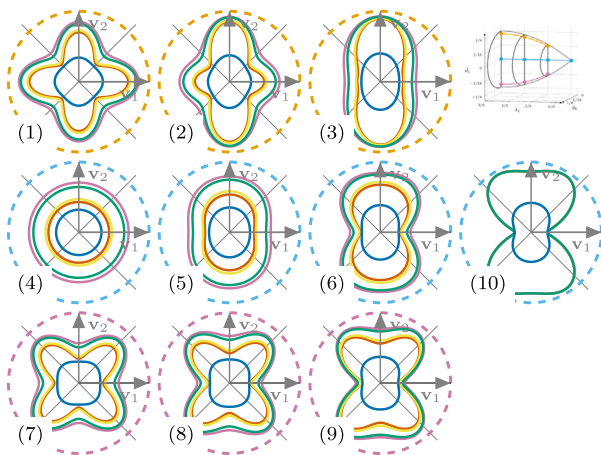
$$G_{16} = \frac{E_{16} (E_{12} E_{33} - E_{13} E_{23} + E_{22} E_{33} - E_{23}^2)}{b} \quad (\text{F.21})$$

$$G_{22} = -\frac{E_{11} E_{33} E_{66} - E_{13}^2 E_{66} - E_{16}^2 E_{33}}{b} \quad (\text{F.22})$$

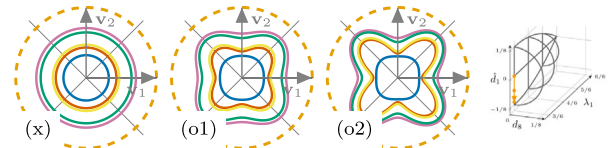
$$G_{23} = \frac{E_{11} E_{23} E_{66} - E_{12} E_{13} E_{66} - E_{13} E_{16}^2 - E_{16}^2 E_{23}}{b} \quad (\text{F.23})$$

$$G_{26} = -\frac{E_{16} (E_{11} E_{33} + E_{12} E_{33} - E_{13}^2 - E_{13} E_{23})}{b} \quad (\text{F.24})$$

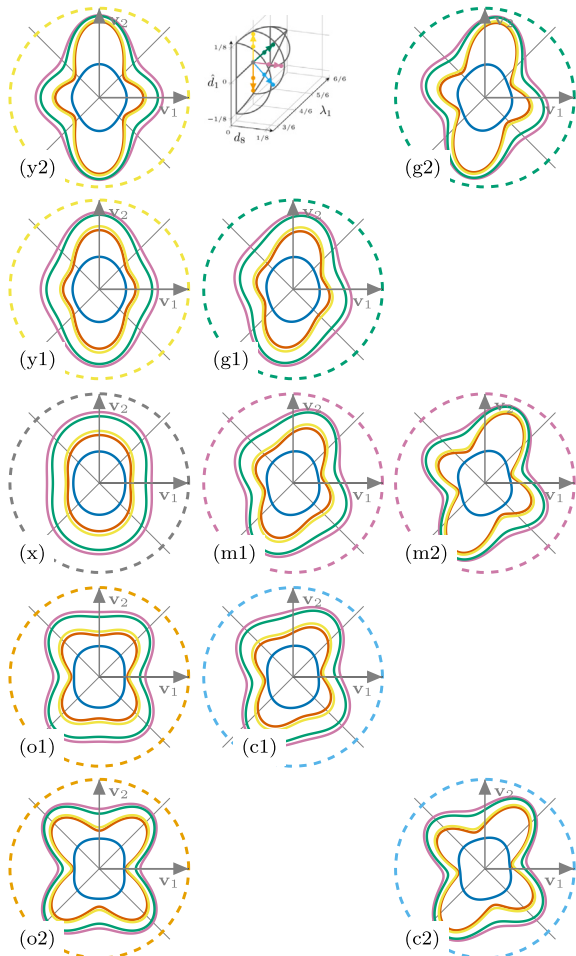
$$G_{33} = \frac{E_{11} E_{16}^2 - E_{11} E_{22} E_{66} + E_{12}^2 E_{66} + 2E_{12} E_{16}^2 + E_{16}^2 E_{22}}{b} \quad (\text{F.25})$$



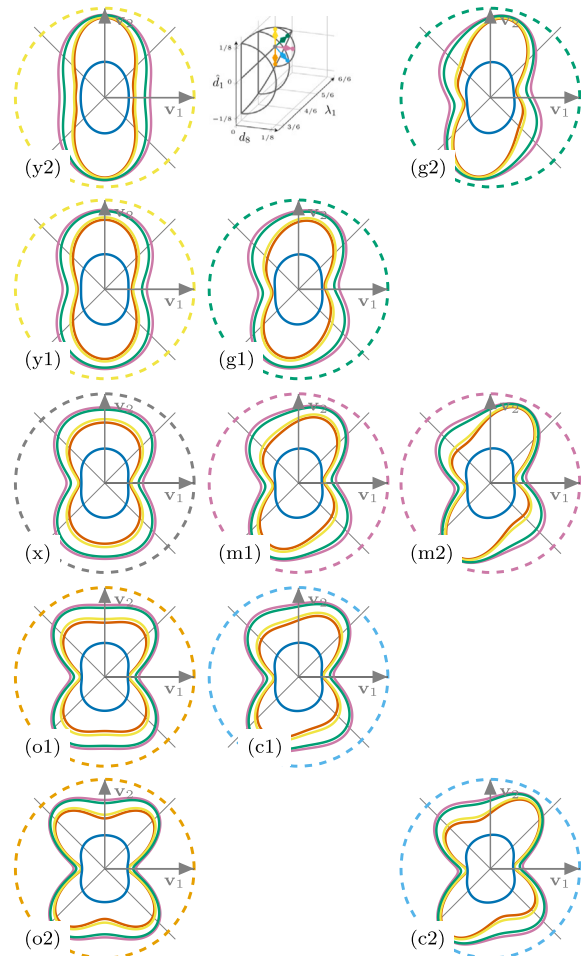
(a) Polar plots for selected N specified in Figure 5a and Table G.2.



(b) Polar plots for selected N with $\lambda_1 = 3/6$ specified in Figure 5b and Table G.2. The order along the path in Figure 5b is given from left to right.



(c) Polar plots for selected N with $\lambda_1 = 4/6$ specified in Figure 6a and Table G.2



(d) Polar plots for selected N with $\lambda_1 = 5/6$ specified in Figure 6b and Table G.2

Fig. H.12. Effective complementary elastic energy $w^*(C, \sigma = 1 \text{ MPa}, n)$ due to uniaxial tension in varying direction defined in Eq. (65) for mean field approximations specified in Fig. 7.

$$G_{36} = \frac{E_{16} (E_{11} E_{23} - E_{12} E_{13} + E_{12} E_{23} - E_{13} E_{22})}{b} \quad (\text{F.26})$$

$$G_{44} = \frac{1}{E_{44}} \quad (\text{F.27})$$

$$G_{55} = \frac{1}{E_{55}} \quad (\text{F.28})$$

$$G_{66} = - \frac{E_{11} E_{22} E_{33} - E_{11} E_{23}^2 - E_{12}^2 E_{33} + 2E_{12} E_{13} E_{23} - E_{13}^2 E_{22}}{b} \quad (\text{F.29})$$

$$b = E_{11} E_{16}^2 E_{33} - E_{11} E_{22} E_{33} E_{66} + E_{11} E_{23}^2 E_{66} + E_{12}^2 E_{33} E_{66} \quad (\text{F.30})$$

$$- 2E_{12} E_{13} E_{23} E_{66} + 2E_{12} E_{16}^2 E_{33} - E_{13}^2 E_{16}^2 + E_{13}^2 E_{22} E_{66} - 2E_{13} E_{16}^2 E_{23} + E_{16}^2 E_{22} E_{33} - E_{16}^2 E_{23}^2 \quad (\text{F.31})$$

Appendix G. Parameter sets in polar plots

Table G.2 lists parameter combinations of all fiber orientation tensors utilized in this work. In addition, Table G.2 contains Lagrange multipliers of the reconstructed fiber orientation distributions.

Appendix H. Effective complementary elastic energy density

Effective complementary elastic energy density due to uniaxial tension with unit stress $\sigma = 1$ MPa defined in Eq. (65) for mean field homogenizations listed in Fig. 7 are given in Figs. H.12(a) to H.12(d). The bounds of the contour plots in Figs. H.12(a) to H.12(d) are homogeneous and given by 0 MJ/m^3 and 0.1 MJ/m^3 .

References

- Advani, S.G., Tucker III, C.L., 1987. The use of tensors to describe and predict fiber orientation in short fiber composites. *J. Rheol.* 31 (8), 751–784.
- Advani, S.G., Tucker III, C.L., 1990. Closure approximations for three-dimensional structure tensors. *J. Rheol.* 34 (3), 367–386.
- Bauer, J.K., 2022. Code accompanying the paper “On the dependence of orientation averaging mean field homogenization on planar fourth-order fiber orientation tensors”. https://github.com/JulianKarlBauer/orientation_averaging_mean_field.
- Bauer, J.K., Böhlke, T., 2021. Variety of fiber orientation tensors. *Math. Mech. Solids* 10812865211057602. <http://dx.doi.org/10.1177/10812865211057602>.
- Bauer, J.K., Böhlke, T., 2022. Fiber orientation distributions based on planar fiber orientation tensors of fourth order. *Math. Mech. Solids* (in Press, to appear).
- Benveniste, Y., 1987. A new approach to the application of Mori-Tanaka's theory in composite materials. *Mech. Mater.* 6 (2), 147–157. [http://dx.doi.org/10.1016/0167-6636\(87\)90005-6](http://dx.doi.org/10.1016/0167-6636(87)90005-6).
- Benveniste, Y., Dvorak, G., Chen, T., 1991. On diagonal and elastic symmetry of the approximate effective stiffness tensor of heterogeneous media. *J. Mech. Phys. Solids* 39 (7), 927–946.
- Bertram, A., Glüge, R., 2013. *Solid Mechanics*. Springer.
- Biegler, M., Mehrabadi, M., 1995. An energy-based constitutive model for anisotropic solids subject to damage. *Mech. Mater.* 19 (2–3), 151–164.
- Böhlke, T., 2001. Crystallographic Texture Evolution and Elastic Anisotropy: Simulation, Modeling, and Applications. Shaker.
- Böhlke, T., Brüggemann, C., 2001. Graphical representation of the generalized Hooke's law. *Tech. Mech.* 21 (2), 145–158.
- Böhlke, T., Henning, F., Hrymak, A., Kärger, L., Weidenmann, K., Wood, J.T., 2019. Continuous–Discontinuous Fiber-Reinforced Polymers: An Integrated Engineering Approach. Carl Hanser Verlag GmbH Co KG.
- Brannon, R.M., 2018. Tensor symmetry (not material symmetry). In: *Rotation, Reflection, and Frame Changes*. 2053–2563. IOP Publishing, ISBN: 978-0-7503-1454-1, pp. 20–21–20–42. <http://dx.doi.org/10.1088/978-0-7503-1454-1ch20>.
- Brylka, B., 2017. Charakterisierung und Modellierung der Steifigkeit von langfaserverstärktem Polypropylen, vol. 10. KIT Scientific Publishing.
- Buck, F., Brylka, B., Müller, V., Müller, T., Weidenmann, K.A., Hrymak, A.N., Henning, F., Böhlke, T., 2015. Two-scale structural mechanical modeling of long fiber reinforced thermoplastics. *Compos. Sci. Technol.* 117, 159–167.
- Camacho, C.W., Tucker III, C.L., Yalvaç, S., McGee, R.L., 1990. Stiffness and thermal expansion predictions for hybrid short fiber composites. *Polym. Compos.* 11 (4), 229–239.
- Chung, D.H., Kwon, T.H., 2002. Invariant-based optimal fitting closure approximation for the numerical prediction of flow-induced fiber orientation. *J. Rheol.* 46 (1), 169–194.
- Cintra, Jr., J.S., Tucker III, C.L., 1995. Orthotropic closure approximations for flow-induced fiber orientation. *J. Rheol.* 39 (6), 1095–1122.
- Cowin, S.C., 1985. The relationship between the elasticity tensor and the fabric tensor. *Mech. Mater.* 4 (2), 137–147.
- Cowin, S.C., Cardoso, L., 2011. Fabric dependence of wave propagation in anisotropic porous media. *Biomech. Model. Mechanobiol.* 10 (1), 39–65.
- Cowin, S., Mehrabadi, M., 1992. The structure of the linear anisotropic elastic symmetries. *J. Mech. Phys. Solids* 40 (7), 1459–1471.
- Cowin, S.C., Van Buskirk, W.C., 1986. Thermodynamic restrictions on the elastic constants of bone. *J. Biomech.* 19 (1), 85–87.
- Eshelby, J.D., 1957. The determination of the elastic field of an ellipsoidal inclusion, and related problems. *Proc. R. Soc. A* 241 (1226), 376–396.
- Fernández, M.L., Böhlke, T., 2019. Representation of Hashin–Shtrikman bounds in terms of texture coefficients for arbitrarily anisotropic polycrystalline materials. *J. Elasticity* 134 (1), 1–38.
- Forté, S., Vianello, M., 1996. Symmetry classes for elasticity tensors. *J. Elasticity* 43 (2), 81–108.
- Goldberg, N., Ospald, F., Schneider, M., 2017. A fiber orientation-adapted integration scheme for computing the hyperelastic tucker average for short fiber reinforced composites. *Comput. Mech.* 60 (4), 595–611.
- Görthofer, J., Meyer, N., Pallicity, T.D., Schöttl, L., Trauth, A., Schemmann, M., Hohberg, M., Pinter, P., Elsner, P., Henning, F., et al., 2019. Virtual process chain of sheet molding compound: Development, validation and perspectives. *Composites B* 169, 133–147.
- Görthofer, J., Schneider, M., Ospald, F., Hrymak, A., Böhlke, T., 2020. Computational homogenization of sheet molding compound composites based on high fidelity representative volume elements. *Comput. Mater. Sci.* 174, 109456.
- Han, K.H., Im, Y.T., 1999. Modified hybrid closure approximation for prediction of flow-induced fiber orientation. *J. Rheol.* 43 (3), 569–589.
- Harris, C.R., Millman, K.J., van der Walt, S.J., et al., 2020. Array programming with NumPy. *Nature* 585 (7825), 357–362. <http://dx.doi.org/10.1038/s41586-020-2649-2>.
- He, Q.-C., Curnier, A., 1995. A more fundamental approach to damaged elastic stress–strain relations. *Int. J. Solids Struct.* 32 (10), 1433–1457.
- Heller, B.P., Smith, D.E., Jack, D.A., Computing mechanical properties from orientation tensor for fiber filled polymers in axisymmetric flow and planar deposition flow. In: *SPE ACCE Conference*. pp. 1–13.
- Hessman, P.A., Welschinger, F., Hornberger, K., Böhlke, T., 2021. On mean field homogenization schemes for short fiber reinforced composites: Unified formulation, application and benchmark. *Int. J. Solids Struct.* 111141.
- Hill, R., 1965. Continuum micro-mechanics of elastoplastic polycrystals. *J. Mech. Phys. Solids* 13 (2), 89–101.
- Hine, P.J., Lusti, H.R., Gusev, A.A., 2004. On the possibility of reduced variable predictions for the thermoelastic properties of short fibre composites. *Compos. Sci. Technol.* 64 (7–8), 1081–1088.
- Iorga, L., Pan, Y., Pelegrí, A., 2008. Numerical characterization of material elastic properties for random fiber composites. *J. Mech. Mater. Struct.* 3 (7), 1279–1298.
- Jack, D.A., Smith, D.E., 2008. Elastic properties of short-fiber polymer composites, derivation and demonstration of analytical forms for expectation and variance from orientation tensors. *J. Compos. Mater.* 42 (3), 277–308.
- Kanatani, K.I., 1984. Distribution of directional data and fabric tensors. *Internat. J. Engrg. Sci.* 22 (2), 149–164. [http://dx.doi.org/10.1016/0020-7225\(84\)90090-9](http://dx.doi.org/10.1016/0020-7225(84)90090-9).
- Karl, T., Gatti, D., Böhlke, T., Frohnappfel, B., 2021. Coupled simulation of flow-induced viscous and elastic anisotropy of short-fiber reinforced composites. *Acta Mech.* 232 (6), 2249–2268.
- Kehrer, M.L., 2019. Thermomechanical Mean-Field Modeling and Experimental Characterization of Long Fiber-Reinforced Sheet Molding Compound Composites. vol. 15. KIT Scientific Publishing.
- Kehrer, L., Wood, J.T., Böhlke, T., 2020. Mean-field homogenization of thermoelastic material properties of a long fiber-reinforced thermoset and experimental investigation. *J. Compos. Mater.* 0021998320920695.
- Köbler, J., Schneider, M., Ospald, F., Andrä, H., Müller, R., 2018. Fiber orientation interpolation for the multiscale analysis of short fiber reinforced composite parts. *Comput. Mech.* 61 (6), 729–750.
- Krylov, V.I., Stroud, A.H., 2006. *Approximate Calculation of Integrals*. Courier Corporation.
- Lielens, G., Pirrotte, P., Couniot, A., Dupret, F., Keunings, R., 1998. Prediction of thermo-mechanical properties for compression moulded composites. *Composites A* 29 (1–2), 63–70.
- Lobos, M., Yuzbasioglu, T., Böhlke, T., 2017. Homogenization and materials design of anisotropic multiphase linear elastic materials using central model functions. *J. Elasticity* 128 (1), 17–60.
- Lubarda, V., Chen, M., 2008. On the elastic moduli and compliances of transversely isotropic and orthotropic materials. *J. Mech. Mater. Struct.* 3 (1), 153–171.
- Mandel, J., 1965. Généralisation de la théorie de plasticité de WT Koiter. *Int. J. Solids Struct.* 1 (3), 273–295.
- Mehrabadi, M.M., Cowin, S.C., 1990. Eigensensors of linear anisotropic elastic materials. *Quart. J. Mech. Appl. Math.* 43 (1), 15–41.
- Meurer, A., Smith, C.P., Paprocki, M., Čertík, O., Kirpichev, S.B., Rocklin, M., Kumar, A., Ivanov, S., Moore, J.K., Singh, S., et al., 2017. Sympy: Symbolic computing in Python. *PeerJ Comput. Sci.* 3, e103.
- Meyer, N., Schöttl, L., Bretz, L., Hrymak, A., Kärger, L., 2020. Direct bundle simulation approach for the compression molding process of sheet molding compound. *Composites A* 132, 105809.
- Montgomery-Smith, S., He, W., Jack, D.A., Smith, D.E., 2011. Exact tensor closures for the three-dimensional Jeffery's equation. *J. Fluid Mech.* 680, 321–335.
- Mori, T., Tanaka, K., 1973. Average stress in matrix and average elastic energy of materials with misfitting inclusions. *Acta Metall.* 21 (5), 571–574.
- Müller, V., 2016. *Micromechanical Modeling of Short-Fiber Reinforced Composites*, vol. 6. KIT Scientific Publishing.
- Müller, V., Böhlke, T., 2016. Prediction of effective elastic properties of fiber reinforced composites using fiber orientation tensors. *Compos. Sci. Technol.* 130, 36–45.
- Nordmann, J., Aßmus, M., Glüge, R., Altenbach, H., 2020. On the derivation of Hooke's law for plane state conditions. *Tech. Mech. Eur. J. Eng. Mech.* 40 (2), 160–174.
- Olive, M., Kolev, B., Desmorat, B., Desmorat, R., 2018. Harmonic factorization and reconstruction of the elasticity tensor. *J. Elasticity* 132 (1), 67–101.
- Pinter, P., Dietrich, S., Bertram, B., Kehrer, L., Elsner, P., Weidenmann, K.A., 2018. Comparison and error estimation of 3D fibre orientation analysis of computed tomography image data for fibre reinforced composites. *NDT E Int.* 95, 26–35.

- Qiu, Y., Weng, G., 1990. On the application of Mori-Tanaka's theory involving transversely isotropic spheroidal inclusions. *Internat. J. Engrg. Sci.* 28 (11), 1121–1137.
- Rychlewski, J., 1984. On Hooke's law. *J. Appl. Math. Mech.* 48 (3), 303–314.
- Rychlewski, J., 2000. A qualitative approach to Hooke's tensors. part I. *Arch. Mech.* 52 (4–5), 737–759.
- Schemmann, M., Gajek, S., Böhlke, T., 2018a. Biaxial tensile tests and microstructure-based inverse parameter identification of inhomogeneous SMC composites. In: *Advances in Mechanics of Materials and Structural Analysis*. Springer, pp. 329–342.
- Schemmann, M., Görthofer, J., Seelig, T., Hrymak, A., Böhlke, T., 2018b. Anisotropic meanfield modeling of debonding and matrix damage in SMC composites. *Compos. Sci. Technol.* 161, 143–158.
- Schjødt-Thomsen, J., Pyrz, R., 2001. The mori-tanaka stiffness tensor: Diagonal symmetry, complex fibre orientations and non-dilute volume fractions. *Mech. Mater.* 33 (10), 531–544.
- Schöttl, L., Dörr, D., Pinter, P., Weidenmann, K.A., Elsner, P., Kärger, L., 2020. A novel approach for segmenting and mapping of local fiber orientation of continuous fiber-reinforced composite laminates based on volumetric images. *NDT E Int.* 110, 102194.
- Schöttl, L., Weidenmann, K.A., Sabiston, T., Inal, K., Elsner, P., 2021. Fiber bundle tracking method to analyze sheet molding compound microstructure based on computed tomography images. *NDT E Int.* 117, 102370.
- Schröder, J., Gross, D., 2004. Invariant formulation of the electromechanical enthalpy function of transversely isotropic piezoelectric materials. *Arch. Appl. Mech.* 73 (8), 533–552.
- Smith, M., 2019. ABAQUS/Standard User's Manual, Version 2019. Dassault Systèmes Simulia Corp, United States.
- Spencer, A., 1970. A note on the decomposition of tensors into traceless symmetric tensors. *Internat. J. Engrg. Sci.* 8 (6), 475–481.
- Spencer, A., 1982. The formulation of constitutive equation for anisotropic solids. In: *Mechanical Behavior of Anisotropic Solids/Comportment Mécanique des Solides Anisotropes*. Springer, pp. 3–26.
- Thomson, W., 1856. Elements of a mathematical theory of elasticity. *Philos. Trans. R. Soc. Lond.* 146, 481–498.
- Trauth, A., Kehrer, L., Pinter, P., Weidenmann, K., Böhlke, T., 2021. On the effective elastic properties based on mean-field homogenization of sheet molding compound composites. *Composites C* 100089.
- Turner, C.H., Cowin, S.C., 1987. Dependence of elastic constants of an anisotropic porous material upon porosity and fabric. *J. Mater. Sci.* 22 (9), 3178–3184.
- Vannucci, P., 2018. *Anisotropic Elasticity*. Springer, Singapore, ISBN: 978-981-10-5438-9.
- Walpole, L., 1966a. On bounds for the overall elastic moduli of inhomogeneous systems—I. *J. Mech. Phys. Solids* 14 (3), 151–162.
- Walpole, L., 1966b. On bounds for the overall elastic moduli of inhomogeneous systems—II. *J. Mech. Phys. Solids* 14 (5), 289–301.
- Walpole, L., 1969. On the overall elastic moduli of composite materials. *J. Mech. Phys. Solids* 17 (4), 235–251.
- Weng, G., 1990. The theoretical connection between Mori-Tanaka's theory and the Hashin-Shtrikman-Walpole bounds. *Internat. J. Engrg. Sci.* 28 (11), 1111–1120.
- Willis, J.R., 1977. Bounds and self-consistent estimates for the overall properties of anisotropic composites. *J. Mech. Phys. Solids* 25 (3), 185–202.
- Willis, J.R., 1981. Variational and related methods for the overall properties of composites. In: *Advances in Applied Mechanics*, vol. 21, Elsevier, pp. 1–78.